AQUEOUS EXTRACTION OF As_2O_3 FROM GIANT MINE ROASTER WASTE AND CHARACTERIZATION OF THE RESIDUES

JILLIAN ABRAHAM

Thesis submitted to the University of Ottawa
in partial fulfillment of the requirements for the
MSc in Earth Science

Department of Earth and Environmental Science
Faculty of Science
University of Ottawa

© Jillian Abraham, Ottawa, Canada, 2026

Abstract

The Giant Mine, located near Yellowknife, NWT, produced over 220 tonnes of gold (Au) from 1948-1999. The ore roasting process created over 237,000 tonnes of As_2O_3–containing roaster waste (ATRW) in the form of dust that is stored in underground chambers. Current plans are to freeze the surrounding ground to prevent groundwater leaching of As_2O_3 into nearby Great Slave Lake. Freezing requires constant maintenance, so this research explores a potentially maintenance-free, safe and permanent alternative. The overall objective is to chemically alter As_2O_3 into a thermodynamically-stable, low-solubility As_2S_3 that could be disposed of safely, deep in the underground mine workings. Specific objectives addressed in this paper are 1) aqueous extraction of As_2O_3 from the ATRW which is necessary prior to sulfidation and 2) characterization of the extraction residues. Extractions were conducted in pure water with a microwave at water-solid ratios ranging from 20-100 and temperatures from 140 °C – 220 °C. The residues were characterized with chemical and x-ray analytical techniques. Complete extraction of the As_2O_3 was accomplished at all temperatures using a water-solid ratio of 100, but small amounts (< 10%) of As_2O_3 remained at lower ratios. In extractions with full As_2O_3 dissolution, residues contain ~1-14 wt% As. Synchrotron (XANES and XRD) analyses of these residues indicate that As is present predominantly as As(V) with lesser As(III), associated with iron (Fe) minerals including goethite, maghemite and hematite. The research demonstrates that complete extraction of As_2O_3 from the waste is possible in water at temperatures ranging from 140 °C– 220 °C. The resulting aqueous As is then amenable to sulfidation to form As_2S_3.

Acknowledgments

This thesis would not have been possible without Dr. Tom Al. I feel incredibly privileged to have been able to work under Tom for the past four years and would like to thank him for everything that he has taught me and for always believing in me, I couldn't have asked for a better supervisor and mentor. The skills and knowledge that he has taught me will forever benefit me as a scientist.

In addition, I would like to thank Tom's research team including Dominique Bower, Guadalupe Maldonado Sanchez and Samuel Morfin for their mentorship and support throughout my research experiences. The lab practises that they taught me were put to great use during my master's degree.

Thank you to Evelyn Tennant and Lianna Smith for their previous research that directly contributed to the groundwork for this thesis and to the personnel of the x-ray core facility, aqueous geochemistry lab at the University of Ottawa and the Canadian Light Source at the University of Saskatchewan – this thesis would not have been possible without all of you. Special thanks to Valerie Schoepfer for not only being a collaborator, but also an incredible friend. Your academic and non-academic advice is appreciated more than you know.

I would like to thank my family, Darlene Abraham (mom), Richard Abraham (dad), Justine Abraham (sister) and Rian Mcgrouther (brother-in-law) for your unwavering support throughout my academic studies. I could not have completed this master's degree without all of you. Thank you, mom, for all of the emotional support phone calls and always encouraging me to do my best while putting myself first. Dad, thank you for passing on your passion for STEM and always being there for me. Justine, thank you for inspiring me to pursue graduate studies and for all your help throughout my academic journey.

Thank you to my friends, Lauren O'Reilly, Rachel Butcher and Jay Miller for everything.

Funding for this research was provided by the Giant Mine Oversight Board (GMOB) and the Canadian Natural Science and Engineering Research Council (NSERC) through the Alliance-Advantage program.

Part of the research described in this paper was performed using beamlines CMCF-BM and BioXAS at the Canadian Light Source, a national research facility of the University of Saskatchewan, which is supported by the Canada Foundation for Innovation (CFI), the Natural Sciences and Engineering Research Council (NSERC), the National Research Council (NRC), the Canadian Institutes of Health Research (CIHR), the Government of Saskatchewan, and the University of Saskatchewan (Fodje et al., 2014).

Table of Contents

List of Tables

List of Figures

1 Introduction

Arsenic (As) occurs naturally in a variety of mineral forms, commonly associated with Fe, Cu, Co, Ni, S, Se, Sb and Te. In Earth's crust, iron (Fe) sulf-arsenides such as arsenopyrite [FeAsS] are likely the most common forms of As (Ali and Ahmed, 2003). The weathering of arsenopyrite causes the formation of As-rich Fe oxyhydroxides (Nickson et al., 1998) which can be eroded and transported through waterways and distributed in sedimentary deposits. These deposits commonly form aquifers and anoxic conditions at depth may lead to reductive dissolution and release of As to groundwater (Nickson et al., 1998). Groundwater supplies 25% of Canada's drinking water (Government of Canada, 2017) and As is commonly detected with an average concentration less than 0.005 mg/L and the maximum acceptable concentration of As in Canadian drinking water supplies is 0.010 mg/L (Health Canada, 2025). In some cases, unregulated drinking water contains higher As concentrations that may pose serious health risks. For example, some aquifers in Bangladesh are naturally contaminated with very high concentrations of As (Yunus et al., 2016).

Arsenic can be released to the environment through various anthropogenic activities (Murcott, 2012). The anthropogenic production of As in the environment begins with extraction of As-containing geologic material from the Earth, which, during processing, may cause As to be distributed in the environment (Han et al., 2003). The extraction and burning of As-containing petroleum and coal, respectively, is responsible for 46% of annual global As production, with the majority produced through mining processes (Han et al., 2003).

Mining of metals such as gold (Au) and silver (Ag) can lead to As environmental contamination. In some ore deposits, Au occurs as fine inclusions in arsenopyrite which is referred to as refractory ore (Jamieson, 2014). To recover the Au, the arsenopyrite can be destroyed by roasting with air in a furnace at high temperatures (Fraser et al., 1991; Qin et al., 2021). Arsenic trioxide (As_2O_3) is a waste product from this process and has previously been released to the environment with roaster gas emissions (Jamieson, 2014;

Bromstad et al., 2017), collected and sold as a wood preservative or environmental pesticide (Moore and Ramamoorthy, 2012; Rae, 2020), or stored in waste impoundments (Clark and Raven, 2004; Bailey et al., 2021). Two notable examples of mining operations that produced particularly large amounts of As_2O_3 are the Giant gold Mine near Yellowknife, NWT, Canada (237,000 tonnes; Jamieson, 2014) and a copper mine and smelter complex in Tsumeb, Namibia (300,000 tonnes; York & Schlaefli, 2025).

Environmental As contamination poses a threat to human health. Arsenic is highly toxic and has been linked to various types of cancer and diseases, including lung, kidney and skin cancer as well as blackfoot disease and central nervous system alterations severely impairing learning and memory abilities (Rodríguez et al., 2003). Various case studies detail the toxic effects of As; one of the most well-known examples is the natural As contamination of aquifers in Bangladesh that resulted in mass poisonings in regions of the population (Yunus et al., 2016). Examples of environmental contamination from mining are common and have resulted in documented human-health effects. For example, people living near a copper smelter operating in Namibia often feel burning sensations in their eyes, throats with a metallic taste in their mouths due to As_2O_3 dust inhalation (York and Schlaefli, 2025). In 1951, a tragic incident happened near the Giant Mine in Yellowknife, NWT when a two-year-old indigenous child died from As poisoning due to atmospheric releases of As_2O_3 dust from an Au processing plant (Sandlos and Keeling, 2016).

Arsenic trioxide is one of the most toxic forms of As due to its high bio accessibility (Jamieson, 2014) and relatively high solubility in water at 25 °C and neutral pH compared to other common As-containing minerals (Dutrizac et al., 2000). Literature values of As_2O_3 solubility at 25 °C have been reviewed by Nordstrom et al. (2014) who report a solubility of 0.207 mol As/kgw which increases with temperature (Dutrizac et al., 2000; Nordstrom et al., 2014).

The Giant Mine produced 220 tonnes of Au and 237,000 tonnes of As_2O_3-containing roaster waste (ATRW) during 51 years of operation (1948 – 1999) (Jamieson, 2014). It is located 5 km North of Yellowknife, Northwest Territories (Figure 1). It is an orogenic deposit located in the Yellowknife

Supergroup of the Canadian Shield, containing quartz-carbonate veins, low sulfide and high As and antimony (Sb) concentrations (Jamieson, 2014).

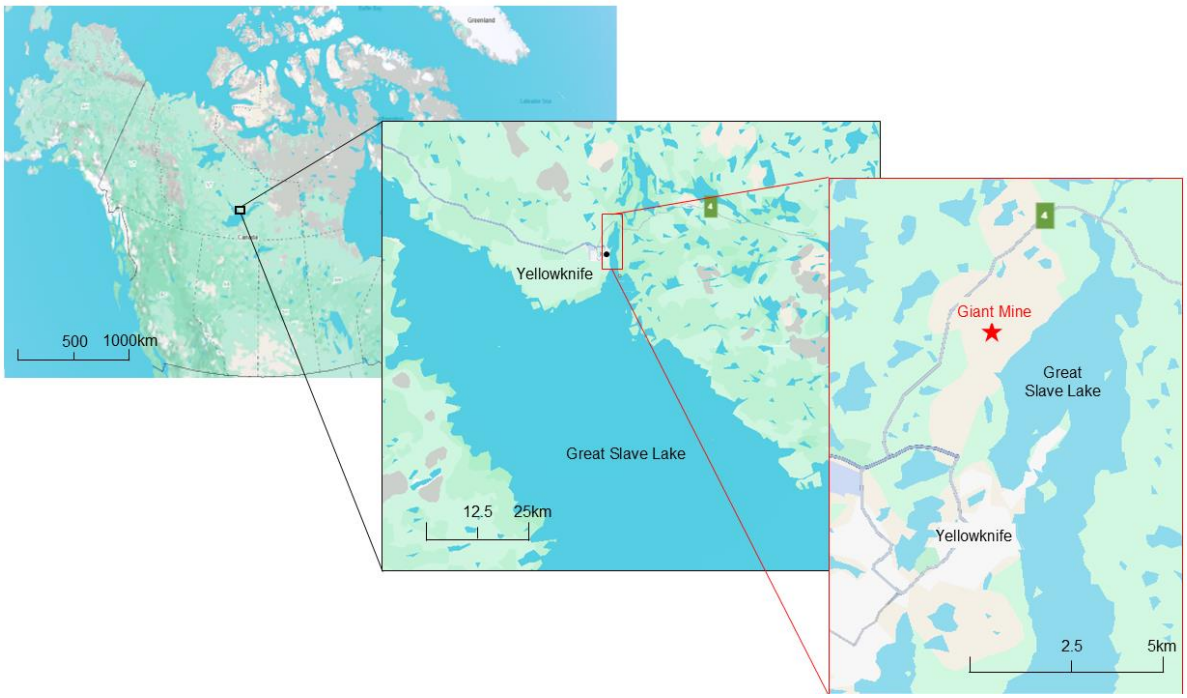

Figure 1. Location of the Giant Mine.

The Au recovery provided revenue of approximately $4.9 billion in 2025 Canadian dollars (INAC and Government of the Northwest Territories, 2010; Bank of Canada, 2025). The ATRW dust was released to the environment during the first three years of mine operation, until collection methods were implemented in 1951. Collection continued for the remainder of the mine life and the ATRW was stored underground in mined-out stopes and purpose-built chambers. The ATRW stored underground poses a significant As-contamination risk to groundwater which flows to nearby Great Slave Lake - one of the largest lakes in North America (INAC and Government of the Northwest Territories, 2010).

Currently, groundwater at the Giant Mine is pumped continually to 10 m below the 750 level (INAC and Government of the Northwest Territories, 2010) (~232 m below ground surface) (SRKb, 2002) to prevent interaction of groundwater with the ATRW. The groundwater is discharged into the northwest tailings

pond and from there to a treatment plant that operates during the summer to remove approximately 98% of the As using hydrogen-peroxide to oxidize Fe and coprecipitate As with ferric hydroxide (SRKa, 2002). The treated water is discharged into Baker Creek (SRKa, 2002) that flows to Great Slave Lake. This is a not suitable long-term solution for storage of the ATRW, so there has been ongoing discussion since the mine closed in 1999 to identify a better management technique.

Crown Indigenous Relations and Northern Affairs Canada (CIRNAC) is the responsible party for decisions related to the mine rehabilitation. After technical assessments and various proposed methods (Table 1), they decided a suitable method would be to freeze the bedrock and contained groundwater that surround the ATRW storage chambers and stopes, to prevent As_2O_3 from entering surrounding groundwater. They refer to this as the frozen block method. That decision led to an environmental impact assessment (EIA) by the Mackenzie Valley Environmental Impact Review Board (Mackenzie Valley Review Board, 2013). The EIA panel decided that freezing was not a suitable permanent solution, so they instructed CIRNAC to fund an oversight body (Giant Mine Oversight Board - GMOB) to be responsible for conducting research into emerging technologies that could provide a permanent remedial option.

Table 1. Brief descriptions of remediation options considered for ATRW at Giant Mine (SRKa, 2002).

	Brief Description
In situ	Contaminated groundwater collection and treatment
	Freezing the rock volume surrounding chambers and stopes
	Removal of the ATRW and disposal underground at the base of the mine
Ex situ	Removal of ATRW and disposal at an off-site hazardous waste facility
	Removal of ATRW, recover Au and make high-purity As
	Removal of ATRW to recover Au and stabilize the As
	Removal of ATRW and stabilize using cementation or vitrification

The frozen block method focused on installing thermosyphons that will operate passively in the winter and actively in the summer to freeze the ground surrounding the chambers and stopes (Zueter and Sasmito, 2023). This method was deemed the safest option because it has the lowest risk of harming workers and the community and minimizes the release of As overtime (Crown-Indigenous Relations and Northern Affairs Canada, 2024).

The GMOB was initiated in 2015 and has been exploring various permanent remediation methods for the ATRW stored at the Giant Mine. For example, current research has been exploring the viability of removing the ATRW from underground and encapsulating it in cemented paste backfill or transforming it to a glass using a vitrification process. The research reported in this thesis is supported by GMOB and explores the possibility to stabilize As from the ATRW by transforming it to As_2S_3.

1.1 Objectives

The overall objective is to chemically alter the As_2O_3 contained in the ATRW to thermodynamically-stable, low-solubility As_2S_3 that could be disposed of safely, deep in the underground mine workings. Specific objectives addressed in this paper are 1) define conditions for dissolving As_2O_3 from the ATRW which is necessary prior to sulfidation 2) minimize the reagents required for the dissolution 3) characterize the mineralogy and chemical composition of extraction solutions and residues.

1.2 Thesis Structure

This thesis has been written in article format, where the body of the thesis represents an independent manuscript intended to be submitted for publication.

Chapter 2 describes the methods, results and discussion of the research objectives and is authored by Jillian Abraham, Lianna Smith, Valerie Schoepfer and Tom Al. Experimental planning and aqueous extraction methodology was completed by Lianna Smith and Tom Al. Lianna Smith completed some initial aqueous extractions. Valerie Schoepfer led the sample preparation, collection and analysis of all x-ray absorption spectroscopy data, with assistance from Jillian Abraham and Tom Al. Jillian Abraham

completed the majority of the sample preparation, experimental operations, data collection, analysis, interpretation and the writing of this thesis with the assistance of Tom Al and personnel in the University of Ottawa geochemistry lab and x-ray core facility.

2 Aqueous extraction of As_2O_3 from Giant Mine roaster waste and characterization of the residues

2.1 Introduction

Mining of metals such as Au, Ag, Cu, Ni and Co may lead to elevated concentrations of arsenic (As) in the surrounding environment due to processing of As-mineral-bearing ores and weathering of As-bearing minerals in tailings and waste-rock impoundments (Ko et al., 2003; Murcott, 2012; Thienpont et al., 2016; Lee et al., 2019; Li et al., 2022). Arsenic is commonly present in wastewater and in drainage from tailings and waste-rock. It can be removed by precipitation reactions with lime [$Ca(OH)_2$] or ferric iron (FeIII) to form calcium-arsenate [$Ca_3(AsO_4)_2$] or Fe oxyhydroxides containing adsorbed As(V) (Riveros et al., 2001). Another alternative is to form scorodite [$FeAsO_4 \cdot 2H_2O$], which has a lower Fe:As ratio and requires a higher energy input and less Fe (Riveros et al., 2001). Arsenic sulfide [As_2S_3] could also be precipitated from As-contaminated wastewater by the addition of H_2S gas (Nazari et al., 2017).

Removal of As from wastewater by precipitation of As-bearing solids is common practice, but the long-term stability of the solids must be considered to ensure As is not released back to the environment over time. For example, calcium-arsenate is unstable over time and dissolves to form calcium carbonate and aqueous AsO_4^{3-} when exposed to atmospheric CO_2, which makes it unsuitable for long term As storage (Riveros et al., 2001). Scorodite and Fe oxyhydroxides containing adsorbed As(V) are also unstable in regions of the natural environment where reducing conditions prevail, but they can be stable when stored in slightly acidic and oxidizing conditions (Riveros et al., 2001). In contrast, As_2S_3 is not stable when exposed to O_2 (Lengke and Tempel, 2002), so long term stability would require an anerobic environment.

In many ore deposits, Au occurs as fine inclusions in the sulf-arsenide mineral, arsenopyrite [FeAsS] – referred to as refractory ore (Jamieson, 2014). To recover the Au, the minerals are destroyed by oxidation using an aqueous pressure-oxidation system (Deng, 1993; Ng et al., 2023; Lemos et al., 2025) or by roasting with air in a furnace fueled by the exothermic oxidation of S and As (Fraser et al., 1991; Qin et al., 2021). Arsenic is a waste product from both processes, and most pressure-oxidation systems create a

ferric-arsenate solid waste (Ng et al., 2023). Similar to scorodite and As-bearing Fe oxyhydroxides precipitated from wastewater, ferric arsenate wastes from pressure oxidation must be stored in a mildly acidic, oxidizing environment to ensure long-term stability. Roasting of refractory ores creates a solid As_2O_3 waste product. Two notable examples of mining operations that produced particularly large amounts of As_2O_3 are the Giant gold mine in Yellowknife, NWT, Canada (237,000 tonnes; Jamieson, 2014) and a copper mine and smelter complex in Tsumeb, Namibia (300,000 tonnes; York & Schlaefli, 2025).

Historically, As_2O_3 waste from roasting has been released to the environment with roaster gas emissions (Bromstad et al., 2017), collected and sold as a wood preservative or environmental pesticide (Moore and Ramamoorthy, 2012; Rae, 2020), or stored in waste impoundments (Clark and Raven, 2004; Bailey et al., 2021). In an attempt to stabilize As_2O_3, Kyle & Lunt, (1991) dissolved it in water and precipitated ferric arsenate using lime neutralization or ferric sulphate (Riveros et al., 2001) but the process was not economically feasible because of the large amount of reagents required. At the Con Mine in Yellowknife, NWT, Canada, As_2O_3 dust (30%) was combined with roaster calcine waste (30%) and Au-rich arsenopyrite concentrate (40%), then processed by pressure oxidation in an autoclave. This allowed for satisfactory Au recovery and precipitation of As in scorodite (Geldart et al., 1992). Cement encapsulation has also been explored to stabilize As_2O_3 at mine sites, with little success. In a recent study, Mohammadi et al. (2024a) created a cement paste backfill (CPB) using a mixture of 6% Portland cement at a 76 wt% solid content, the solids consisting of 10 wt% of Giant Mine As_2O_3 containing roaster waste (ATRW). The mixtures were cured for 28 days before conducting leaching tests. They found that 41% of As leached out of the CPB – demonstrating that incorporating As_2O_3 in cemented paste backfill or some other cemented encapsulation system would create a long-term contamination risk (Mohammadi et al., 2024b).

Arsenic trioxide is one of the most toxic forms of As, due to its high bio accessibility (Jamieson, 2014) and relatively high solubility in water at 25 °C and neutral pH (Table 2) compared to other common As

minerals (Dutrizac et al., 2000). Literature values for As_2O_3 solubility at 25 °C in water have been reviewed by Nordstrom et al. (2014) who report a solubility of 0.207 mol As/kgw or 15.49 g As/kgw. Arsenic trioxide solubility increases with temperature (Pokrovski et al., 1996; Nordstrom et al., 2014) and in alkaline solutions (Ali and Ahmed, 2003). Solubility versus temperature (0 – 250 °C) from three different studies are presented in Figure 2.

Table 2. Solubility of common As minerals in water determined using PHREEQC (wateq4f database) (Ball and Nordstrom, 1991) at 25°C and pH of 7. References are for the original solubility product constant.

As Mineral	Solubility (g As/kgw)	Reference
Arsenolite [As_2O_3]	15.22	NBS Technical Notes 270 (Wagman and others, 1968, 1969; Parker and others, 1971)
Scorodite [$FeAsO_4 \cdot 2H_2O$]	0.0435	Naumov and others (1974)
Realgar [As_4S_4]	0.000404	Naumov and others (1974)
Orpiment [As_2S_3]	0.00568	NBS Technical Notes 270 (Wagman and others, 1968, 1969; Parker and others, 1971)

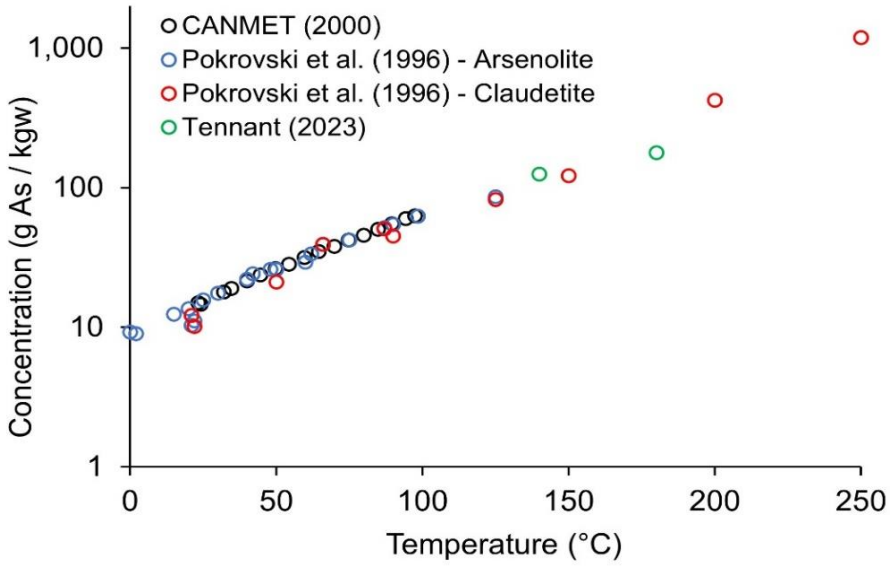

Figure 2. Solubility of As_2O_3 in water at various temperatures; adapted from multiple sources.

The Giant Mine is located 5 km North of Yellowknife, Northwest Territories (NWT) (Figure 3). It produced over 220 tonnes of Au during its operation from 1948 – 1999 (Jamieson, 2014). It is an orogenic deposit located in the Yellowknife Supergroup of the Canadian Shield, containing quartz-carbonate veins, low sulfide and high As and antimony (Sb) concentrations (Jamieson, 2014). The ore is refractory, meaning that most of the Au occurs as inclusions in arsenopyrite.

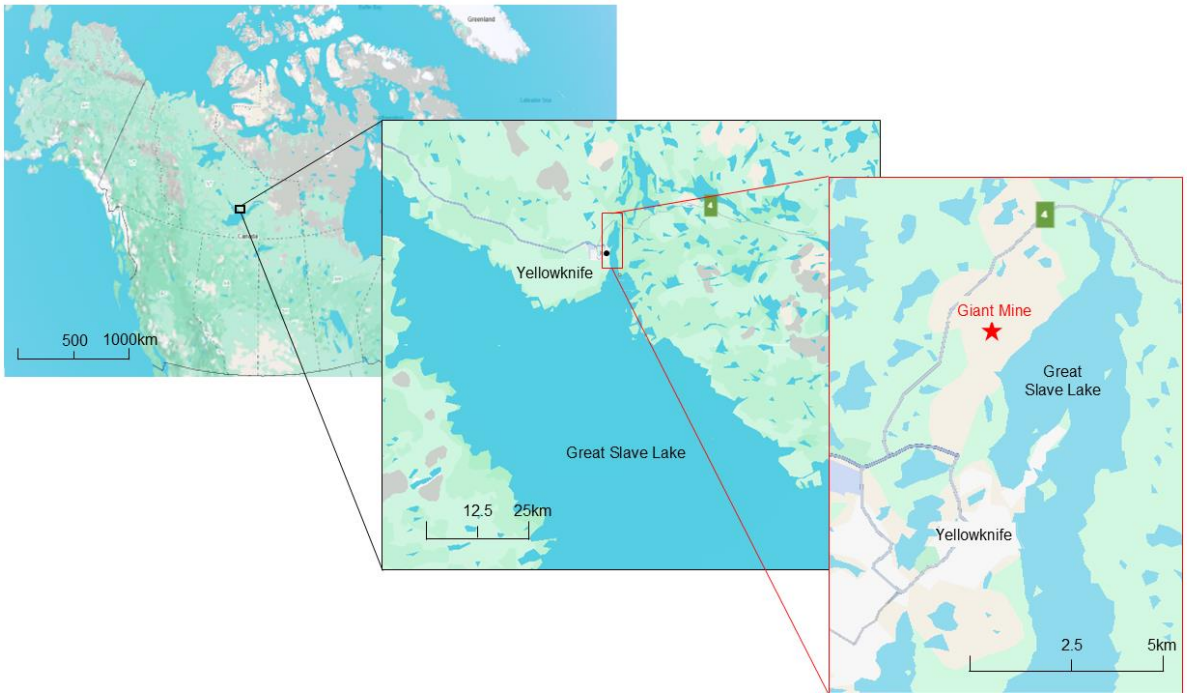

Figure 3. Giant Mine location.

The Au recovery process began by crushing and grinding the ore until 80% is less than 200 mesh followed by flotation to concentrate Au-containing arsenopyrite. The arsenopyrite was oxidatively destroyed (roasted) at temperatures of 450 to 500 °C to liberate the Au for subsequent recovery. Roasting created an Au-rich Fe oxide (calcine) which was ground in a ball mill and sent to a cyanide leach circuit where the Au was recovered from solution using a Merrill-Crowe precipitation process (Northwest Consulting Limited, 2003). Arsenic released as a gas during roasting was condensed and recovered as

As_2O_3, with a total of 237,000 tonnes of arsenic-trioxide-containing roaster waste (ATRW) accumulated during the life of the mine (Bromstad and Jamieson, 2012).

The ATRW is currently stored underground at a maximum depth of 76 m in 10 purpose-built chambers and five mined out stopes at the Giant Mine site (SRK, 2007) (Figure 4, Figure 5). The water table is lowered by pumping, but if the area was allowed to reflood the natural water table would sit 1-2 m below ground surface (SRKb, 2002) with increasing elevation inland from Great Slave Lake, which would cause flow toward the lake.

Figure 4. Map showing the Giant Mine site near Yellowknife, NWT, Canada (left) and ATRW storage locations in white shapes (right). The ATRW used in this study was derived from locations highlighted in yellow. Modified after Lum et al. (2023).

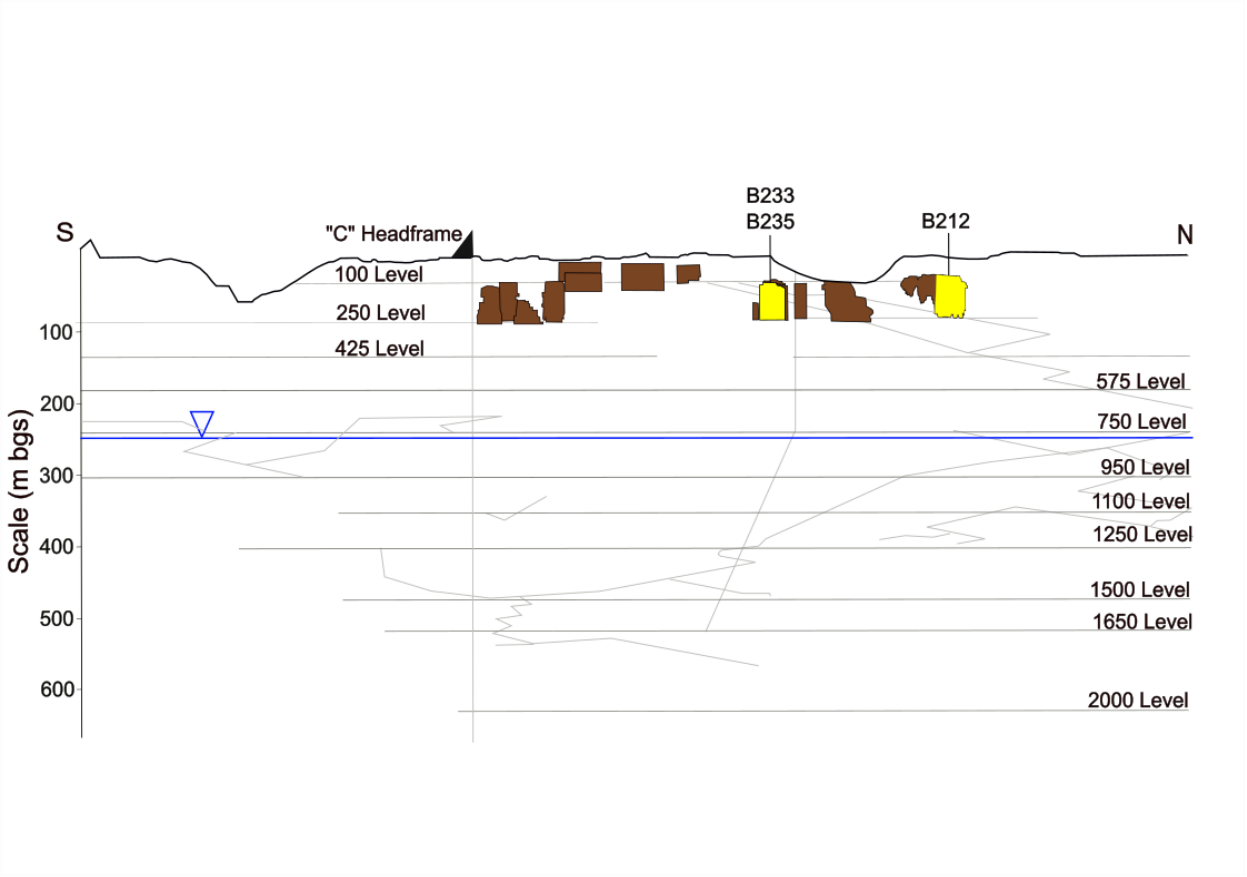

Figure 5. Distribution of ATRW chambers and stopes. Chambers B233 and B235 overlap and are highlighted closer to the South, stope B212 is highlighted farthest to the North. The current water table is shown in blue. Figure adapted from Royal Oak Mines (1997).

Arsenic trioxide roaster waste contains various minerals, dominantly arsenolite [As_2O_3] with minor amounts of Fe oxides, Fe arsenate, chlorite, muscovite and quartz (Dutrizac et al., 2000). Lum et al. (2023) determined that As(III) is dominant, with some As(V) and minor amounts of As associated with Fe oxides including maghemite and hematite. Walker et al. (2015) report similar results, with maghemite and lesser hematite (plus adsorbed As) being the dominant Fe oxides. Lum et al. (2023) also reported the occurrence of Sb(III) and Sb(V), with Sb(III) substituted in As_2O_3 and stibioclaudetite [$AsSbO_3$].

The overall objective is to chemically alter the As_2O_3 contained in the ATRW to thermodynamically-stable, low-solubility As_2S_3 that could be disposed of safely, deep in the underground mine workings. Specific objectives addressed in this paper are 1) define conditions for dissolving As_2O_3 from the ATRW which is necessary prior to sulfidation 2) minimize the reagents required for the dissolution 3) characterize the mineralogy and chemical composition of extraction solutions and residues.

2.2 Methods

2.2.1 Sample Selection

Samples of ATRW from Giant Mine were provided by the GMOB from archived materials held at SGS - Canada in Lakefield, Ontario. The goal was to choose a subset of materials that were representative of the range of chemical compositions exhibited by the Giant Mine waste. Samples from chambers B212, B235 and B233 were chosen because, based on compositional data from MacGregor et al. (2004), material from these chambers represented a large range of As, Sb and Fe concentrations which are the principal components in the Giant Mine ATRW (Table 3).

Table 3. Concentrations of As, Sb and Fe in ATRW from chambers B212, B235 and B233.

Element (%)	B212	B235	B233
As	60.2	66	39.5
Sb	1.7	0.37	1.8
Fe	2.5	2.0	15

2.2.2 Aqueous extraction of As_2O_3 from ATRW

Roaster waste solids containing As_2O_3 were weighed into a teflon-lined 35 mL glass vial and extractions were conducted with de-ionized water using a microwave (CEM Discover 2.0) at variable water-solid (W:S) mass ratios (20, 40, 60, 80, 100) typically using 200 mg of ATRW and 20 g of deionized water for 100 W:S ratio, temperatures (140, 160, 180, 200, 220 °C), and times (one and four minutes). To the extent possible, temperature was held constant for a designated extraction time, but additional sample heating

occurs prior to, and following, the designated time during the heating and cooling periods (Figure 6a). The system pressure varies with temperature, approximately corresponding to the equilibrium liquid – vapour curve of the water phase diagram (Figure 6b).

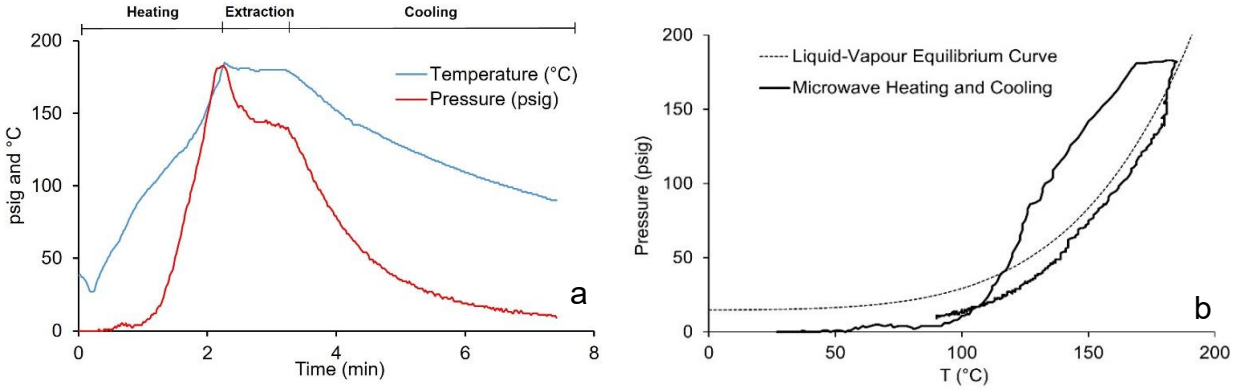

Figure 6. (a) Temperature and pressure variation versus time in microwave showing heating, extraction and cooling periods (b) Microwave pressure during heating and cooling corresponding to the liquid-vapour equilibrium curve of the water phase diagram.

The aqueous extraction vials were removed from the microwave, rinsed into a centrifuge tube, and immediately diluted (dilution factor ≈ 2). The tube was centrifuged at 3200 rpm for 50 minutes and then the extraction solution was removed from the centrifuge tube, filtered (0.2 µm cellulose acetate), acidified using trace-metal-grade concentrated nitric acid and refrigerated. The solid residue was retained in the centrifuge tube and placed in a fume hood to dry for 24 hours.

The solid residues from all extraction experiments were analyzed for the presence of residual As_2O_3 using powder XRD (Bruker D8 Endeavour). Each residue was ground into a fine, homogeneous powder using a mortar and pestle and packed into a zero-background holder (MTI Corporation). The XRD analyses were conducted with Cu K-alpha radiation (λ = 1.54 Å) over a range from 5 to 75° 2Θ with a step size of 0.02 and the integration time was 0.48 s per step. Extraction yield was determined by integrating intensity over a range of 2Θ from 13.56 to 14.06 which is centered on the (111) peak for As_2O_3. The only

known interference in this range for this material is the Sb(III) trioxide, senarmontite [Sb_2O_3]. The integrated intensities from the extraction residues were normalized to the integrated intensity from the raw ATRW peak to obtain an estimate of the fraction of As_2O_3 remaining in the residue. This value is subtracted from one and multiplied by 100% to obtain the extraction yield.

2.2.3 Chemical analysis of extraction solutions

Elemental concentrations were measured in solutions from aqueous As_2O_3 extractions at W:S = 100 (Al, As, Ca, Cu, Fe, K, Mg, Mn, Na, Ni, S, Sb, Si and Zn). Measurements were conducted by inductively-coupled-plasma optical-emission spectrometry (ICP-OES) and accuracy and precision were determined using certified reference materials (CRM) (Table A- 4). The analytical precision (relative standard deviation, RSD) is less than 10% for all elements except Ni (14.7%) and Si (44.8%), and accuracy ranges from 4.1 to 29.6% (Table 4). Arsenic accuracy is relatively high due to the low As concentration in the CRM compared to the high concentration in the extraction solutions.

Table 4. Analytical precision (RSD%) and accuracy for analysis of aqueous As_2O_3 extraction solutions.

Element	Accuracy (%)	Precision (%)
Al	25.1	1.3
As	29.6	8.3
Ca	-2.3	1.6
Cu	7.6	3.3
Fe	-2.8	2.0
K	6.7	1.2
Mg	4.1	1.9
Mn	22.8	1.7
Na	11.4	1.1
Ni	-3.4	14.7
S	6.1	1.9
Sb	25.6	7.6
Si	15.9	44.8
Zn	-4.1	1.9

2.2.4 Characterization of the residue

2.2.4.1 Digestion and chemical analysis

Solid residues from the aqueous extractions (W:S = 100) were digested by adding approximately 1 mL of aqua regia (3:1 ratio of concentrated HCl and HNO_3) to approximately 30 mg of residue. Digestions were conducted in Savillex vials in a 90 °C water bath for 24 hours. This approach does not achieve complete dissolution of all mineral phases, particularly silicates and some aluminosilicates, so Si, Al, Na, Mg and K are not reported.

The resulting solutions were analyzed by ICP-OES for As, Cu, Fe, Mn, Ni, Pb, S, Sb and Zn and accuracy and precision were determined using CRMs (Table A- 4). Accuracy ranges from 2.2 to 22.6% and precision from 0.5 to 7.8% (Table 5).

Table 5. Analytical precision (RSD%) and accuracy for analysis of the digested solid residues.

Element	Accuracy (%)	Precision (%)
As	13.5	7.8
Cu	8.9	0.5
Fe	4.7	1.0
Mn	6.8	0.7
Ni	6.4	0.8
Pb	3.6	1.7
S	2.2	1.1
Sb	22.6	6.0
Zn	8.9	0.8

2.2.4.1.1 Gold analysis

Solid residues from all extractions for chambers B212 and B233 were combined separately and various subsamples from each chamber were digested using aqua regia acid. The resulting solutions were analyzed for Au by inductively-coupled-plasma mass spectrometry (ICP-MS).

2.2.4.2 Synchrotron XRD

Analyses were conducted at the Canadian Macromolecular Crystallography Facility beamline (CMCF-BM) at the Canadian Light Source (CLS) in Saskatoon, Saskatchewan. Residue samples were ground to a fine powder in a mortar and pestle, and sealed in 2.3-cm-long, 0.5 mm diameter Kapton capillary tubes. Each Kapton tube was placed on a goniometer positioned 349.5 mm from the detector (PILATUS3 6M, S/N 60-0136) in a Debye-Sherrer geometry set-up. A camera took digital images as the sample rotated for 120 seconds while exposed to the x-ray beam (λ = 0.6888 Å). The images were transformed to diffractograms using GSAS (version II) (Toby and Von Dreele, 2013) and mineral identification was performed with Bruker DIFFRAC.EVA software and the ICDD-PDF database. DIFFRAC.EVA provides estimates of mineral fractions (%) based on peak-intensity ratios. A LaB_6 reference powder was used for calibration, and an empty capillary tube was analyzed to allow for background subtraction.

2.2.4.3 XAS methods

Analyses were conducted at the Biological X-ray Absorption Spectroscopy (BioXAS) beamline at the CLS. X-ray Absorption Near Edge Spectroscopy (XANES) data were collected around the As, Sb and Fe K-edges for various mineral standards (Table 6). The standards were finely ground in a mortar and pestle and sprinkled on Kapton tape, except for maghemite which was ground with boron nitride in a mortar and pestle and pressed into a pellet.

Table 6. XANES mineral standards.

Mineral Standard	Source	Reference
As_2O_3	Alpha Aesar CAS 1327-52-3	
As_2O_5	Sigma-Aldrich CAS 12044-50-7	
As(V) adsorbed to goethite	Synthesized	Schwertmann and Cornell (2000)
As(III) adsorbed to hematite and maghemite	Natural	Walker et al. (2005)
As(V) scorodite	Synthesized	Rong et al. (2020)
Sb_2O_3	Sigma-Aldrich CAS 1309-64-4	

Sb_2O_5	Sigma-Aldrich CAS 1314-60-9	
Goethite	Synthesized	Schwertmann and Cornell (2000)
Hematite	Synthesized	Schwertmann and Cornell (2000)
Maghemite	Canadian Museum of Nature collection #48683	

Residue samples were finely ground and homogenized in boron nitride using an agate mortar and pestle. The mixture was pressed into pellets, inserted into a sample holder and covered by Kapton tape. Sample holders were plunge frozen in liquid nitrogen, fixed in a cryostat and inserted in the beamline at an angle of 45 degrees to the incident beam (0.5 mm x 3 mm). Transmission and fluorescence data were simultaneously collected during a 30-minute acquisition time. Two or three replicate scans were conducted around the As, Sb and Fe K-edges. For Fe and As, a step size of 5 eV was applied from -200 eV to -30 eV and steps of 0.5 eV were used from -30 eV to 80 eV, relative to the Fe and As K edges (7112 eV and 11,867 eV, respectively). For Sb, a step size of 5 eV was applied from -200 eV to -30 eV and steps of 1.0 eV were used from -30 eV to 40 eV, relative to the Sb K edge (30,491 eV). The energy was selected using a liquid-nitrogen-cooled Si-double-crystal monochromator and the beam was focused using a Rh-coated Si mirror. Fluorescence data were collected by 32-element Ge detectors oriented 90 degrees to the incident beam and 45 degrees to the sample. The signal was improved using filters and soller slits to absorb scattered x-rays. Gas-ionization chambers measured incident (I_0), transmission (I_1) and reference (I_2) intensities and were filled with nitrogen gas (N_2) for As and Fe and argon gas (Ar) for Sb.

Data analysis was performed using Athena Demeter 0.9.26 and Larix Larch version 2025.1.1. Data collected in transmission mode were used for As and Fe data analysis and fluorescence data were used for Sb analysis because the transmission signal was insufficient for reliable quantitation.

Normalization of the data was conducted in Athena by manually selecting pre-edge and post-edge regions of each spectrum to obtain the best fit of a first-order polynomial and second-order polynomial,

respectively. Energy and spectrum alignment were conducted using Au, Sb and Fe reference foils for As, Sb and Fe, respectively.

Linear combination fitting (LCF) was performed in Larch to determine As, Sb and Fe speciation. Mineral standards used for fitting were selected based on visual examination of the spectra and previous knowledge that ATRW contains As_2O_3 with a small fraction of maghemite, hematite and As(V) (Lum et al., 2023). It should be noted that As_2O_3 and As_2O_5 were included in LCF analysis, but their inclusion resulted in a relatively poor fit. All linear combination fits were conducted within a specific energy range (As: 11,830 eV – 11,970 eV, Sb: 30,450 eV – 30,590 eV, Fe: 7085 eV – 7400 eV) without forcing the sum of component weights to 1, and with a maximum E_0 shift of 0.376 eV. The best fit was determined by minimizing the r-squared value. The limit of detection for LCF is +/- 10% (Parsons et al., 2009).

2.3 Results

2.3.1 As_2O_3 extractions

The extraction yield is lowest for ATRW from chamber B212 (Figure 7), but it increases with W:S ratio from a minimum of approximately 91% at W:S ratio of 20 to 100% at W:S ratio of 100. There is one exception with an extraction yield of only 96% at 140 °C and W:S ratio of 100. A similar increase in extraction yield versus W:S ratio is observed for the ATRW from chamber B235 (Figure 7). Compared to the ATRW from chamber B212, the yields are higher (lowest ~98%) and increase to near 100% at W:S > 60. The extraction yields for ATRW obtained from chamber B233 are distinct in that the yields are > 99% for all W:S ratios (Figure 7).

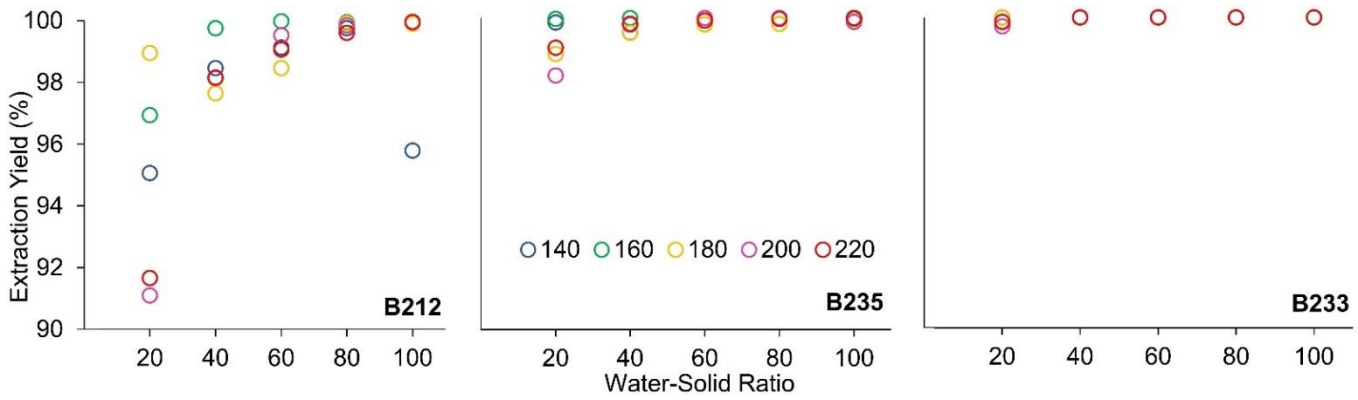

Figure 7. Extraction yield (%) versus W:S ratio for all temperatures and extraction time of one minute.

There is a general trend of increasing extraction yield with temperature for the data from chamber B212 (Figure 8), but there is some inconsistency for W:S ratios of 40 and 60. For chamber B235, the extraction yield was > 99% for the majority of the temperature and W:S ratio conditions; but a decrease in extraction yield of 1 to 2% was observed for the W:S ratio of 20 between 200 and 220 °C (Figure 8). The extraction yields are consistently near 100% for the ATRW from chamber B233 and there are no trends versus temperature (Figure 8).

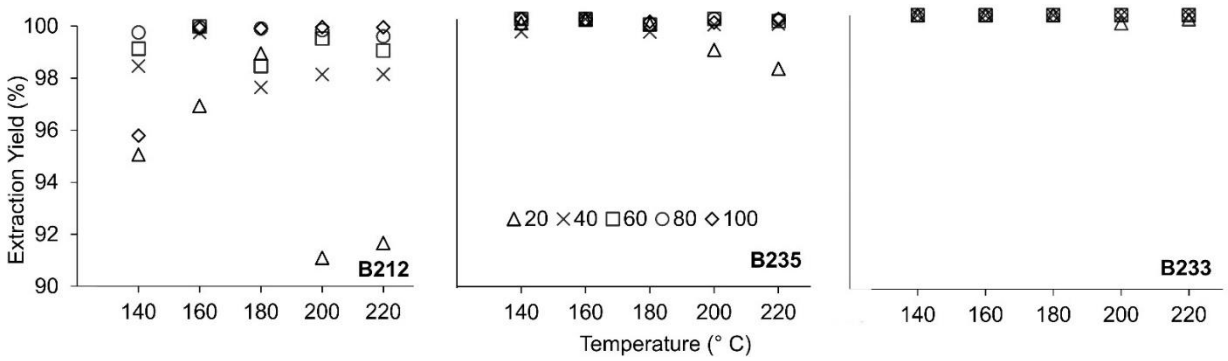

Figure 8. Extraction yield (%) versus temperature (°C) for all W:S ratios and an extraction time of one minute.

The ATRW from chamber B212 was used to test the effect of increased extraction time because this material displayed the lowest extraction yields for the one-minute extraction time. Results indicate that there is no apparent improvement in extraction yield with a four-minute reaction time (Figure 9).

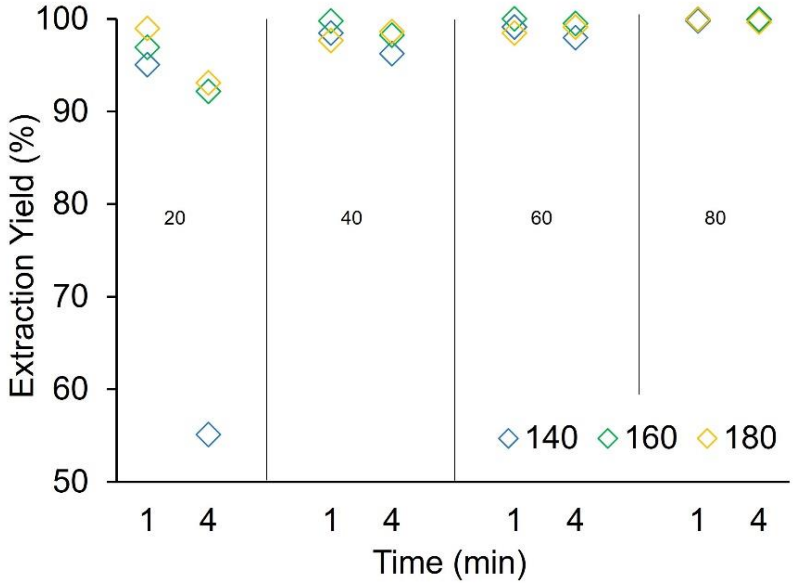

Figure 9. Extraction yield (%) versus time for W:S ranging from 20 to 80 and temperatures of 140, 160 and 180 °C.

2.3.2 Extraction solutions

The average concentrations of As in the solutions are 5808 ppm, 6590 ppm and 3756 ppm, for chambers B212, B235 and B233, respectively and the corresponding average Sb concentrations are 128 ppm, 24 ppm, and 10 ppm (Figure *10*). All other aqueous concentrations are < 50 ppm, except for Ca and S in chamber B233, with concentrations of approximately 53 ppm and 93 ppm, respectively.

There is no apparent trend in As concentration versus temperature. The Sb concentration in solutions from chambers B212 and B233 displays small, but consistent increases with temperature. Similarly, although the concentrations are generally low (< 10 ppm), there are trends of increasing concentration with temperature for Al, Cu, Fe, Mn, Si and Zn.

A key feature of the data is the distinct compositional differences between extraction solutions from chambers B212 and B235 compared to chamber B233. The As and Sb concentrations are relatively high

in solutions for chambers B212 and B235, while concentrations of Al, Cu, Fe, Mn, Ni, S, and Zn are relatively high in solutions from chamber B233.

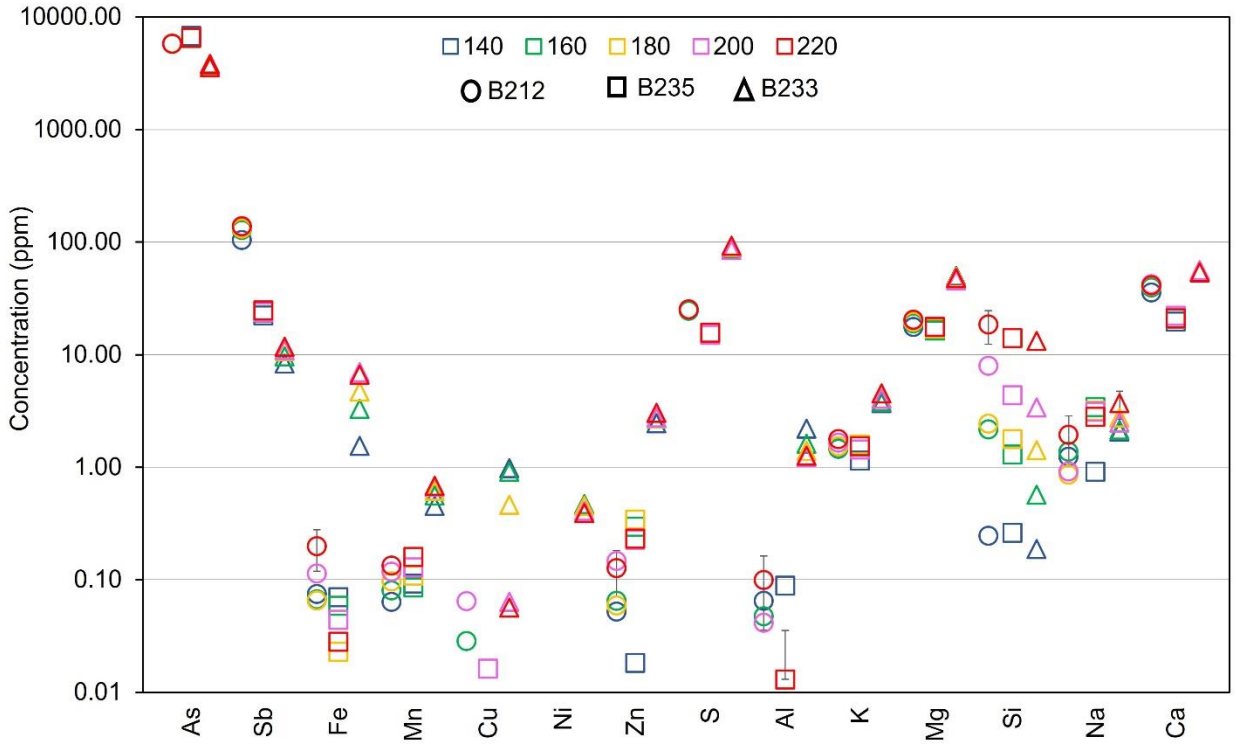

Figure 10. Elemental concentrations in extraction solutions for all temperatures and W:S = 100. Mean values (n=3) are plotted for 220 °C and error bars (+/- 1σ) are only included when larger than symbols.

2.3.3 Residue Characterization

2.3.3.1 Residue Mass

The mass fraction of the ATRW sample that remains as a residue from the aqueous extractions varies among the chambers. The average residual mass fractions from extractions conducted with W:S = 100 are presented in Table 7. They range from 9.2% for chamber B235 to 38% for chamber B233.

Table 7. Average residual mass fraction.

	B212	**B235**	**B233**
Residual mass fraction (%)	20	9.2	38
σ (%) (n=14)	1.3	1.6	2.5

2.3.3.2 Chemical composition

The average As concentrations in the residue are 93,000 ppm, 103,000 ppm and 164,000 ppm for chambers B212, B235 and B233, respectively, and the corresponding average Sb concentrations are 33,000 ppm, 10,000 ppm, and 30,000 ppm (Figure *11*). Average Fe concentrations are 182,000 ppm, 143,000 ppm and 219,000 ppm for chambers B212, B235 and B233, respectively. All other elemental concentrations are < 10,000 ppm and are similar in all chambers. The concentrations of As, Sb and Fe in the residues vary only slightly according to the extraction temperature that each was subjected to.

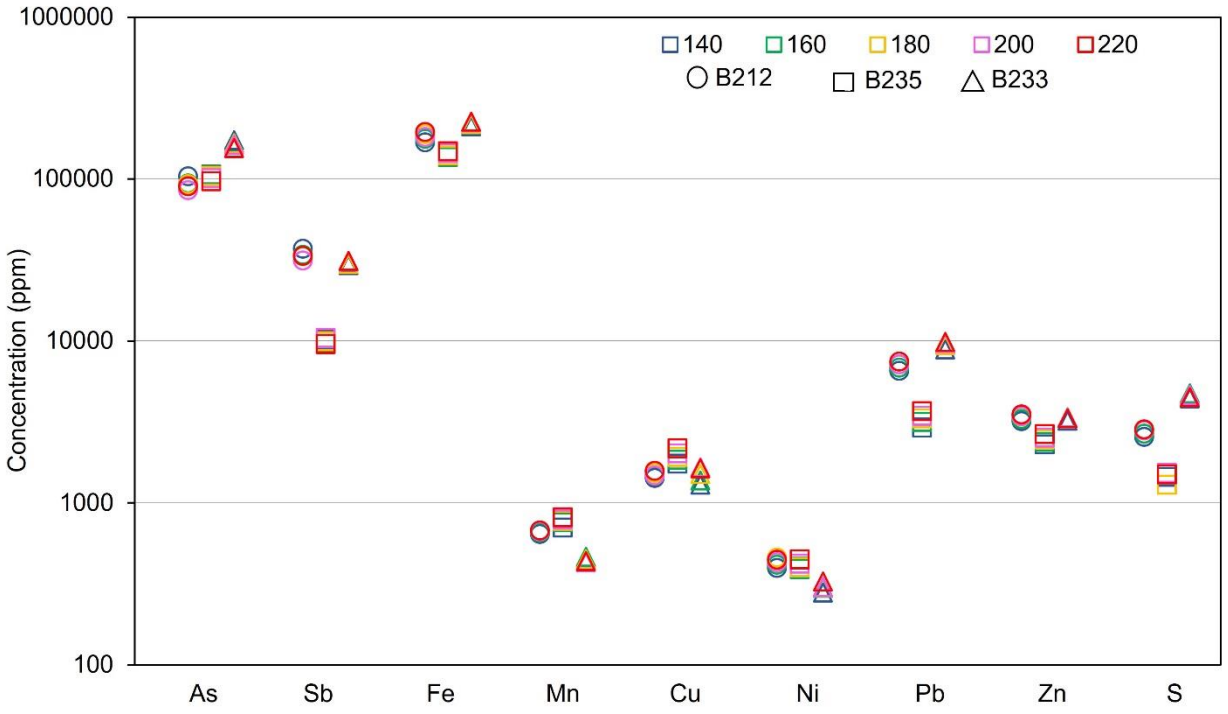

Figure 11. Elemental composition (ppm) of residues from all extraction temperatures and extraction time of one-minute. Mean values (n=3) are plotted for chamber B233, 220 °C and error bars (+/- 1σ) are not included because they are smaller than the symbols.

Gold concentrations in subsamples of extraction residue range from 92.84 ppm to 183.74 ppm for chamber B212 and 70.84 ppm to 166.10 ppm for chamber B233 (Table 8). Both chambers have similar average Au concentrations, 119.45 and 124.45 ppm for chambers B212 and B233, respectively.

Table 8. Gold concentrations (ppm) in residue.

	Au (ppm)	
Subsample	**B212**	**B233**
1	98.89	104.80
2	121.01	166.10
3	183.74	119.48
4	115.26	149.50
5	110.41	144.00
6	117.94	120.07
7	111.29	115.40
8	131.44	127.78
9	113.18	70.84
10	156.37	126.56
11	92.84	
12	97.73	
13	102.78	
Average	119.45	124.45
σ	25.38	26.13

2.3.3.3 Mineralogy

The mineralogical compositions of the residues from extractions completed at 180 °C and a W:S ratio of 100 for one minute are presented in Table 9. Arsenic-bearing phases were detected in residue from chambers B212 and B233, As_2O_3 (~1%) in B233 and scorodite (~5%) in B212. A single Sb-bearing phase, Sb_2O_3, was detected in residue from chamber B212 (<1%). Quartz is the dominant mineral component in residues from all chambers, ranging from 19 to 37% of the material. Residues from chambers B212 and B235 contain a significant amount of $Fe^{(III)}$ - bearing muscovite. Residues from chamber B212 have more maghemite (~25%) than those from chamber B235 (~5%) and half the clinochlore content (~10% versus ~21%). Residues from chamber B233 have a distinctly different mineral composition than residues from chambers B212 and B235 reflected in the lack of chlinochlore, relatively low quartz, and relatively high hematite, maghemite and scorodite content.

Table 9. Estimates for mineral fractions (%) identified through powder x-ray diffraction.

	Chamber		
	B212	**B235**	**B233**
As_2O_3	1		
Clinochlore-1Mlb, $Fe^{(II)}$ bearing	10	21	
Hematite, syn			9
Maghemite, syn	25		45
Maghemite, Ti bearing		5	
Microcline	12		
Muscovite-2M1			22
Muscovite-2M1, $Fe^{(III)}$ bearing	27	37	
Scorodite			5
Sb_2O_3	< 1		
Quartz	25	37	19

2.3.3.4 Solid-phase As, Sb and Fe speciation

The XANES spectra for all residues, including extraction temperatures ranging from 140 – 220 °C, extraction times of one and four minutes, and W:S = 100 are presented in Figure 12. The spectra from each chamber are very similar, displaying almost complete overlap despite differences in extraction temperature and time. For this reason, a subset of residue materials representing extractions conducted at 180 °C, one minute duration and W:S = 100 are used for all subsequent analysis and discussion.

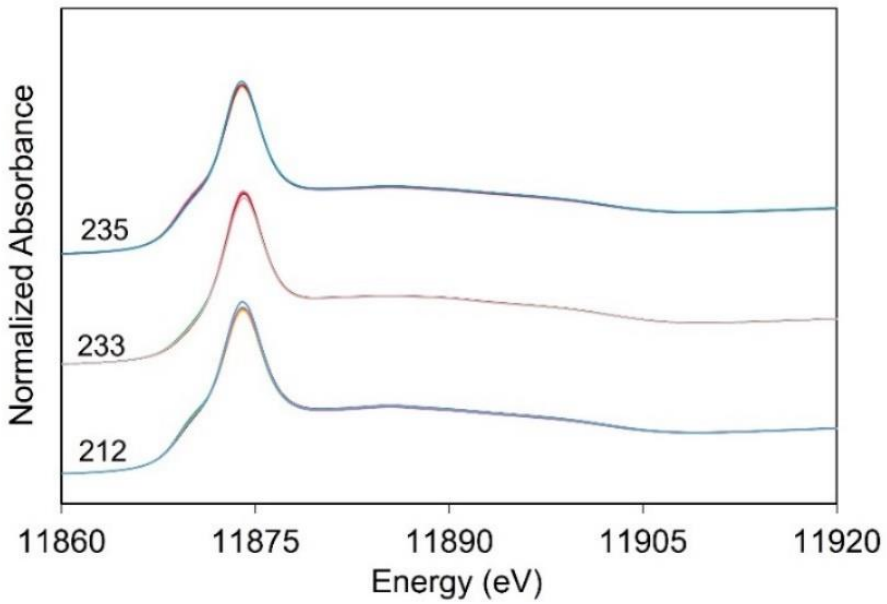

Figure 12. As-K edge XANES spectra for residues from chambers B212, B233 and B235 representing all extraction temperatures, extraction times of one and four minutes and W:S = 100. There are six, five and six individual spectra included for chambers B212, B233 and B235, respectively.

Spectra from chambers B212 and B235 are very similar and display a peak absorbance at 11,874 eV with a small shoulder peak at 11,869 eV (Figure 13), consistent with the absorption peaks for As(V) and As(III), respectively. These data indicate that residual As in the extraction residues occurs dominantly in the As(V) oxidation state, with a lesser component of As(III). The mineral proportions obtained from the linear combination fitting are consistent with this observation, indicating that 77% of the fits are attributable to As(V) adsorbed to goethite and 23% to As(III) adsorbed to hematite and maghemite (Table 10).

In contrast to residues from chambers B212 and B235, spectra for residues from chamber B233 do not display a shoulder peak at 11,869 eV, indicating that As in these residues is dominated by the As(V) oxidation state. This is consistent with the outcome of the linear combination fitting which suggests that 97% of the As is present in the form of scorodite (84%) and As(V) adsorbed to goethite (14%). The fitting

results suggest that the remaining 3% of residual As is present as As(III) adsorbed to hematite and maghemite (Table 10).

Table 10. Results from linear combination fitting of As, Sb and Fe spectra for mineral standards and extraction residues from chambers B212, B235 and B233. Normalized to one post-LCF.

	B212	**B235**	**B233**
Arsenic Species			
As (V) scorodite			0.83
As (V) adsorbed to goethite	0.77	0.77	0.14
As (III) adsorbed to hematite and maghemite	0.23	0.23	0.03
r-factor	0.001183	0.001288	0.000466
Antimony Species			
Sb_2O_3	1.00	1.00	0.89
Sb_2O_5			0.11
r-factor	0.0019	0.0010	0.0011
Iron Species			
Maghemite	0.48	0.42	0.36
Goethite	0.43	0.46	0.22
Scorodite			0.34
Hematite	0.09	0.12	0.08
r-factor	0.0003767	0.0007342	0.0000919

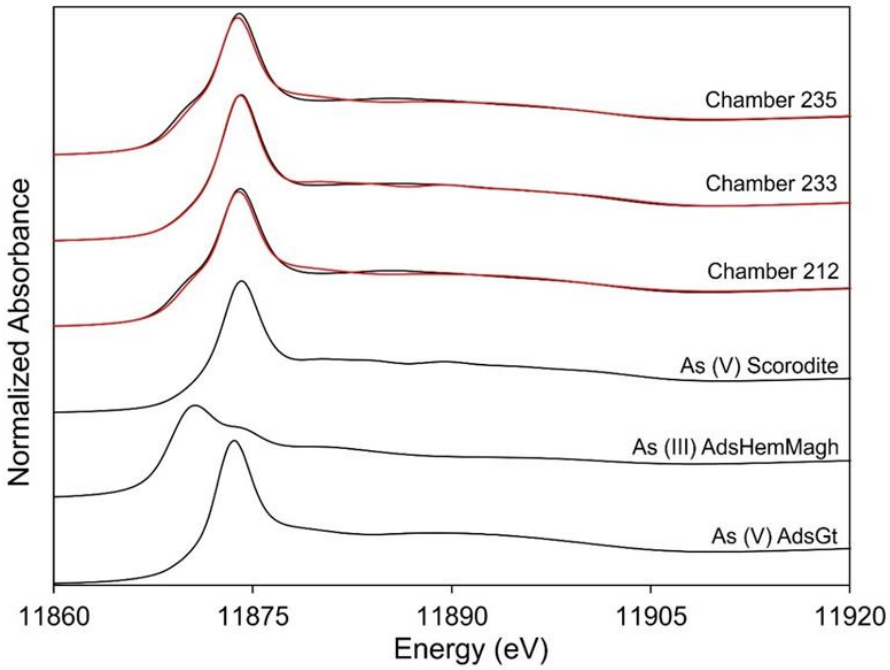

Figure 13. As-K edge XANES spectra for residues from extractions conducted on ATRW from chambers B212, B233 and B235 (180 °C, one minute, W:S = 100). Black lines are the normalized spectra for samples and standards, and red lines are the linear combination best fit.

The Sb XANES spectra for all samples from chambers B212 and B235 (Figure 14) display a peak absorbance at 30,501 eV, which corresponds to the principal peak for Sb_2O_3. The pre- and post-peak regions of the spectra are relatively featureless. The linear combination fits for the Sb spectra are based on only two standards, but the fitting suggests that Sb(III) is 100% dominant in these residues, likely Sb_2O_3 (Table 10).

The spectra for residues from chamber B233 differ from those from chambers B212 and B235 in that the peak absorbance is shifted to a higher energy, consistent with a contribution from Sb(V) (Figure 14). This is reflected in the results for the linear combination fitting which suggest 89% of Sb is present in the Sb(III) oxidation state and 11% in the Sb(V) oxidation state (Table 10).

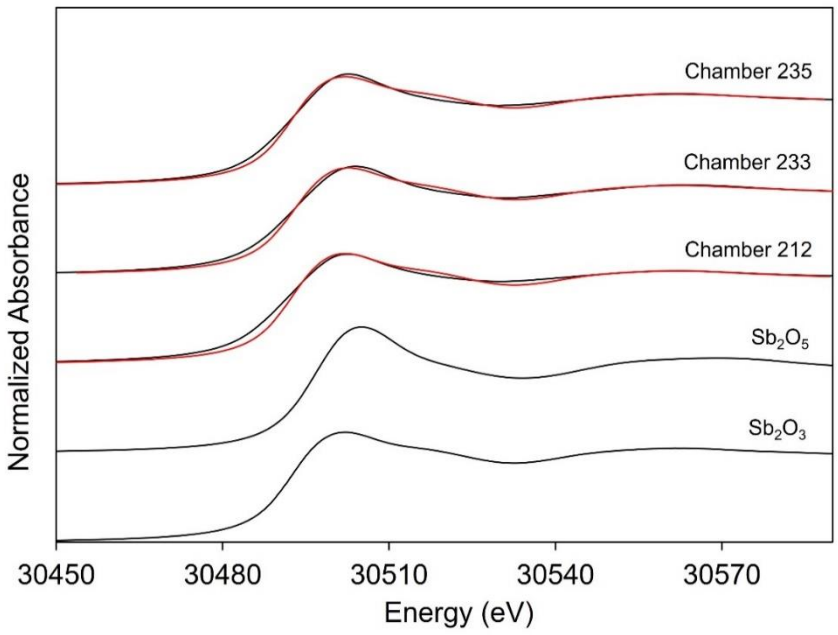

Figure 14. Sb-K edge XANES spectra for residues from extractions conducted on ATRW from chambers B212, B233 and B235 (180 °C, one minute, 100 W:S). Black lines are the normalized spectra, and red lines are the linear combination best fit.

The Fe XANES spectra for residues from all chambers are similar (Figure 15), displaying a peak absorbance at 7133 eV with a small pre-edge peak at 7114 eV. These peak and pre-edge absorbance energies are the same as for the maghemite standard, demonstrating that Fe(III) is dominant. There are slight differences in the spectra for residues from chamber B233 compared to residues from chambers B212 and B235, the principal difference being the appearance of a small peak at ~7138 eV that corresponds with a similar feature in the scorodite spectra. The linear combination fitting suggests that Fe minerals in the residues from chambers B212 and B235 include 42-48% maghemite, 43-46% to goethite and 9-12% hematite (Table 10). In contrast, the derived mineral composition for residues from chamber B233 includes scorodite (34%) with lesser maghemite (36%), goethite (22%) and hematite (8%).

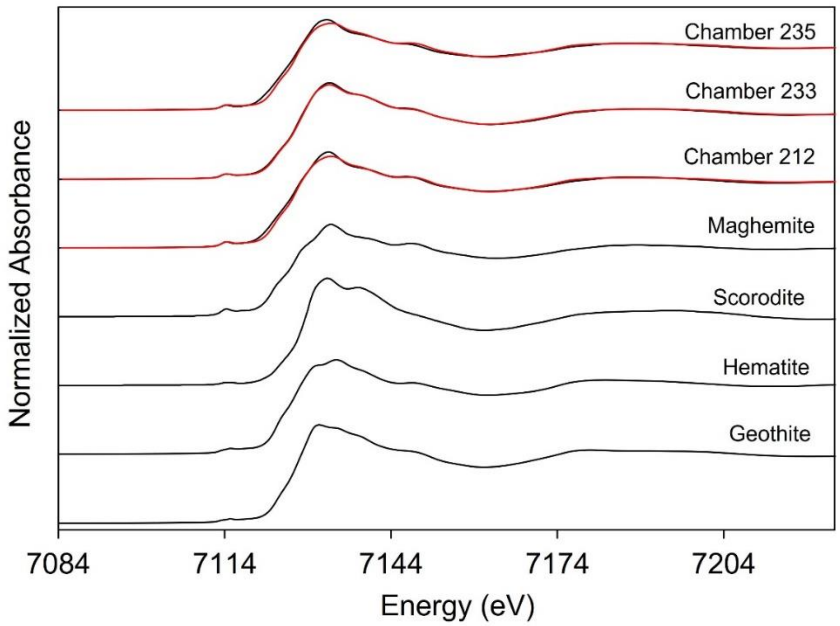

Figure 15. Fe-K edge XANES spectra for residues from extractions conducted on ATRW from chambers B212, B233 and B235 (180 °C, one minute, 100 W:S). Black lines are the normalized spectra, and red lines are the linear combination best fit.

2.3.4 Extractable mass fraction

Quantitative analysis of powder XRD data allowed for estimation of the As_2O_3 extraction yields. The chemical analyses of the extraction solutions and the residues allow for an alternative assessment of As extraction yield based on chemical mass balance. This chemical mass balance is defined here as the extractable mass fraction (EMF) to distinguish it from the extraction yield defined above. It is calculated for individual elements according to:

$$EMF = \frac{mass\ in\ extraction\ solution}{mass\ in\ extraction\ solution\ +\ mass\ in\ residue} \times 100\%$$

The As extractable mass fraction is highest in chamber B235 ATRW, reaching approximately 99% at all temperatures. Similar results are obtained for ATRW from chamber B212, reaching 97% As extractability

with little variability between temperatures. The lowest As extractable mass fraction is 87% for ATRW from chamber B233 (Figure *16*).

Antimony extractable mass fraction increases with temperature ranging from 55% at 140 °C to 70% at 200 °C for ATRW from chamber B212 and from 65% at 140 °C to 77% at 220 °C for ATRW from chamber B235. The ATRW from chamber B233 is unique in that Sb extractability is comparatively low, varying with temperature from 7 to 9% (Figure *16*).

The extractable mass fraction of Fe is relatively low (0.025 to 0.85%) for ATRW from all three chambers at all temperatures (Figure *16*).

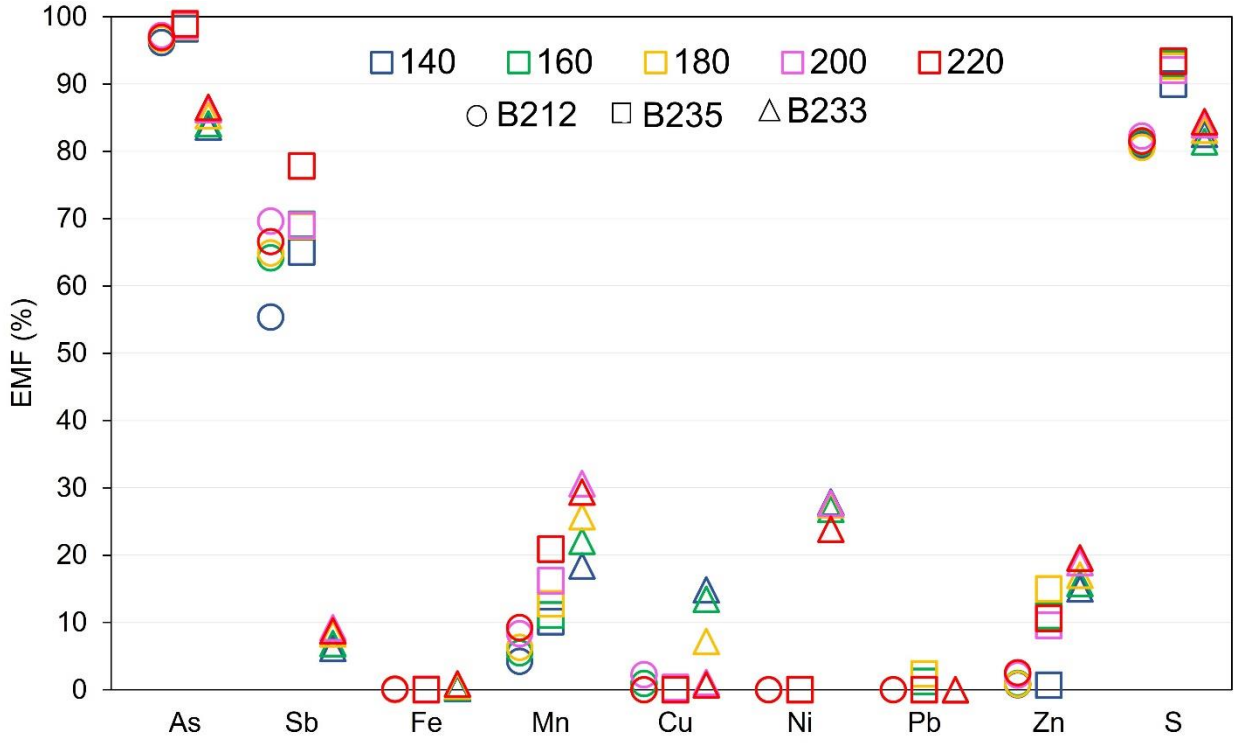

Figure 16. Extractable mass fractions (%) determined for extraction temperatures ranging from 140 °C to 220 °C.

2.4 Discussion

One of the key objectives of this study was to explore methods for extracting As_2O_3 from the ATRW at Giant Mine to facilitate transformation of the As to a more stable form that could be safely and permanently stored with little risk of contaminating the surrounding environment. Our broad objective is to test sulfidation to transform the aqueous As(III) to solid As_2S_3 that could be disposed of permanently deep in the abandoned mine workings, but other transformative reactions could be considered if it can be demonstrated possible to dissolve all of the As_2O_3 in the ATRW. A focus for the current study has been to develop a method to dissolve all of the As_2O_3 while minimizing the need to transport large quantities of reagents to the north which could pose health, safety and environmental risks along the transport routes, and could lead to creation of additional waste streams in the form of spent reagents. The method described in this work uses only water and energy (heat) and virtually complete dissolution of the As_2O_3 is achieved at a W:S ratio of 100. Although pure water is perhaps the simplest of all possible reagents, it would become contaminated by the As_2O_3 extraction process. Analysis of the extraction solutions for a W:S ratio of 100 (Figure *10*) indicates that As is by far the principal component and concentrations of all other elements are much lower. If these solutions were subjected to sulfidation using H_2S, the concentrations of As and other minor components (Cu, Fe, Ni, Pb, Sb and Zn) would be expected to drop below 1 ppm. This would leave a residual aqueous solution containing major ions Ca, Mg, Na, K and SO_4 with combined concentrations < 100 ppm (chambers B212 and B235) and ~200 ppm (chamber B233). These major-ion concentrations are similar to those in some potable groundwater and are sufficiently dilute that the water could be recycled numerous times through the As_2O_3 extraction process, thereby minimizing waste-water generation.

The ATRW at Giant Mine is a mixture comprised of primary minerals from the ore body, Au-bearing Fe-oxide from the roaster (calcine) and As_2O_3. The proportions of these components are variable, so the mass fraction of non-As_2O_3 residue is variable. For the material studied in this work, the residue mass fractions were approximately 20%, 38% and 9.2% for chambers B212, B233 and B235, respectively (Table 7). The estimated total mass of ATRW at Giant Mine is 237,000 tonnes, but there are insufficient data to estimate

the total mass of residue that would remain after extracting all the As_2O_3. For the purpose of discussion, if we assume it is 25%, then there would be approximately 60,000 tonnes of residue. The residue contains Au-rich calcine (Table 8), so at present Au prices it could be considered a valuable commodity. However, it also contains concentrations of As on the order of 93,000 to 164,000 ppm, and depending on the mineral speciation of the As, the residue might also be considered a risk to the environment, and therefore a liability. These pros and cons can only be weighed when there is a good understanding of the material properties, and this was the motivation for studying the residue. In the process, it quickly became apparent that the material properties of the residue are tied to the evolution of the roasting and ATRW-collection processes employed at Giant Mine.

The ore roasting process at the Giant Mine evolved over time with the goal of optimizing Au and As recovery. A flotation concentrate containing arsenopyrite, pyrite [FeS_2], some stibnite [Sb_2S_3], and other vein and wall-rock minerals was roasted at a temperature of 450 to 500 °C (Foster, 1963; Royal Oak Mines, 1995; Northwest Consulting Limited, 2003) to produce Au-bearing calcine that was captured and directed to a Au-recovery circuit. The roaster exhaust gas contained As, Sb and SO_2, along with some escaped dust (calcine and primary minerals from the ore body). In the early days of the mine, no dust-capturing methods were employed, and SO_2 with condensed particles of As_2O_3, Sb_2O_3, calcine and primary-mineral dust were released to the atmosphere via stack emissions. This posed environmental concerns, so a cooling gradient and dust-collection system were added to condense and capture the As in the form of As_2O_3 dust.

The current study demonstrates that the ATRW is not homogeneous and the most obvious variability in material properties is observed between the oldest studied ATRW from chamber B233 compared to later-formed ATRW from chambers B212 and B235. The key observations are:

A. The mass of residue remaining after the aqueous extractions is anomalously large for chamber B233; residual mass fractions are 38%, 20% and 9.2% for B233, B212 and B235 respectively (Table 7).

B. The extraction residues from chamber B233 contain relatively low alumino-silicate content and relatively high Fe-oxide content compared to extraction residues from material in chambers B212 and B235 (Table 9).
C. The extractable mass fractions for As and Sb in ATRW from chamber B233 (87% and 9% respectively) are significantly lower than those for chamber B212 (97% and 55 to 70%, respectively) and chamber B235 (99% and 65 to 77%, respectively) (Figure *16*).
D. The As_2O_3 extraction yield for ATRW from chamber B233 is near 100% across the entire range of W:S ratios and extraction temperatures, whereas the yields are lower for material from chambers B212 and B235 (Figure 7 and Figure 8).
E. The XANES data indicate that As(V) in the extraction residues is dominant, but the spectra indicate a minor component of As(III) in residues from chambers B212 and B233 which is not evident in spectra from chamber B233 (Figure 13).
F. The XANES data suggest Sb(III) in the residues is dominant, except in residues from chamber B233 which contain a minor fraction (~11%) of Sb(V) (Table 10).
G. The XRD and XANES data indicate the occurrence of scorodite only in residue from chamber B233 (Table 9 and Table 10).

Among the three different underground chambers from which ATRW used in this study was sourced, material from chamber B233 is the oldest, B235 second oldest and B212 the youngest (Figure 17). The differences in the material properties likely reflect the evolving roasting and dust-collection processes. The timelines and details of the roaster-circuit evolution in the following discussion are derived from Foster (1963) and company reports by Royal Oak Mines (1995); Northwest Consulting Limited (2003) and MacGregor et al. (2004).

The first stage of dust-collection was implemented in 1951, when an electrostatic precipitator (ESP) was installed in a relatively cool region of the roaster-exhaust-gas circuit (Figure 17). Calcine and primary minerals that escaped the roaster were transported in the cooling gas stream along with mixed As and Sb

vapour and their condensed forms. The solids were collected at the ESP and stored as ATRW. Because Au-rich calcine escaped the roaster, the resulting ATRW had relatively high concentrations of Au and Fe. The two main drawbacks were that Au recovery was low because calcine was lost to the ATRW, and the ESP was not efficient so As_2O_3 dust concentrations in the stack emissions were unacceptably high. Most of the ATRW in chamber B233 was collected during this stage (prior to 1958) which explains the high Fe-oxide-mineral content, the corresponding high residual mass fraction (observations A and B), and the relatively low bulk As content (Table 3).

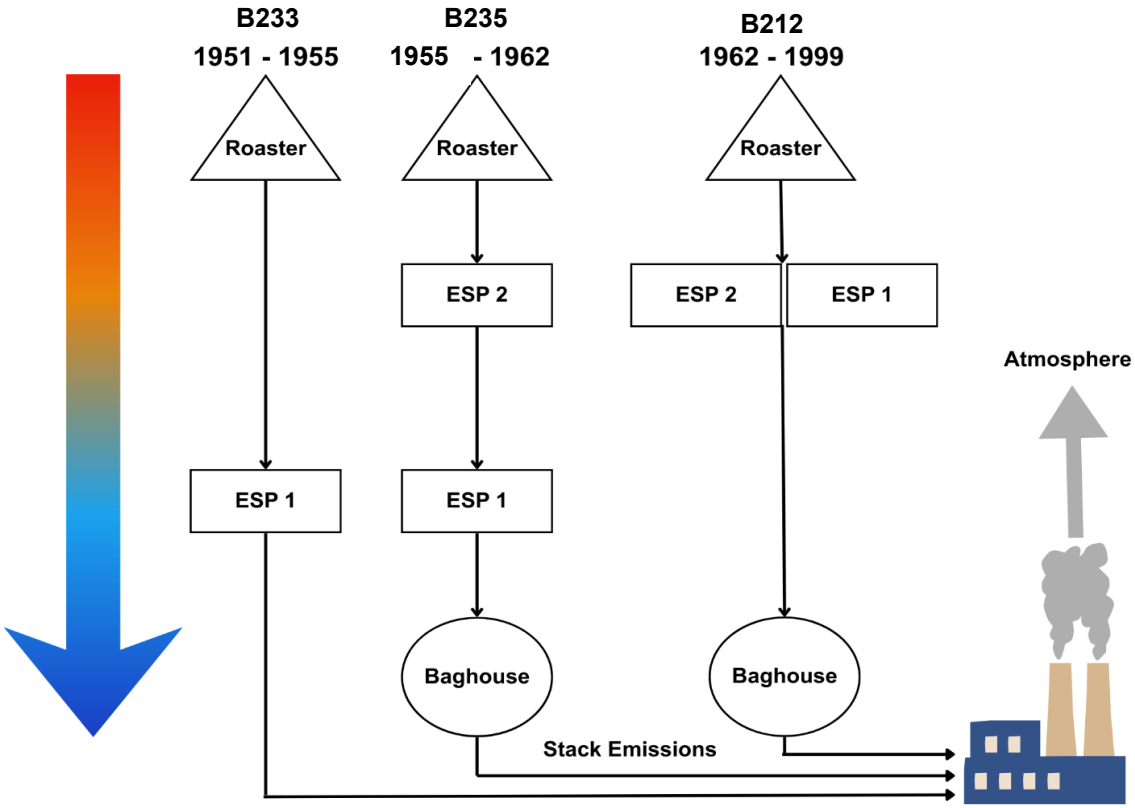

Figure 17. ATRW collection through time. Warm and cool colours represent hot and cold areas of the circuit, respectively. Chamber labels correspond to the ATRW collection process at the time that they were filled.

In 1955, a second ESP was added in the high-temperature region of the gas stream, close to the roaster (Figure 17). The goal was to collect calcine before the As and Sb vapours condensed, thereby separating

the valuable calcine from the ATRW which was captured at the low-temperature ESP. This was successful and the majority of calcine was captured for Au recovery. However, the low-temperature ESP remained inefficient, so As_2O_3 dust concentrations in the stack emissions remained unacceptably high. The solution to this problem came in 1957 when a fabric baghouse was first tested to filter solids from the gas emissions, and in 1958 a full-scale baghouse was installed and As_2O_3 dust emissions were brought to an acceptable level. The ATRW stored in chamber B235 was produced after installation of the second ESP and the baghouse (1958 to 1962). In 1962, both ESPs were moved to the high-temperature region to increase efficiency of calcine collection (Figure 17) and this configuration was used through the remaining life of the mine (Royal Oak Mines, 1995). Chamber B212 was filled between 1973 and 1986.

Several lines of evidence indicate that the disposition of Sb in the ATRW changed after the installation of the second ESP in 1955. This is relevant because it has been suggested that substitution of Sb_2O_3 in As_2O_3 lowers the solubility of the mixed phase relative to pure As_2O_3 (Dutrizac et al., 2000) which could explain the lower As_2O_3 extraction yields for ATRW from chambers B212 and B235 (observation D). The elemental mass-balance data from aqueous extractions (Figure *16*, Table A- 3) demonstrate that the extractable Sb mass fraction increased from 9% for ATRW in chamber B233 to 55 to 77% for ATRW from chambers B212 and B235 (observation C). Given that As_2O_3 extraction yields are consistently highest (~100%) for ATRW from chamber B233 (Figure 7), it follows that most of the Sb mass in ATRW from chamber B233 is associated with phases other than As_2O_3 and that Sb_2O_3 substitution in As_2O_3 is relatively high for ATRW from chambers B212 and B235. The tendency for Sb_2O_3 to partition to the As_2O_3, or to some other solid phase in the ATRW, is likely controlled by the condensation temperature and the amount of solid surface area on which condensation might occur. Tuominen et al. (2025) investigated Sb condensation in conditions representative of smelter gas streams and found condensation temperature varies as a function of O_2 concentration in the gas stream. Over a range of 0.5 to 5 vol% O_2 they noted that most of the Sb condensed and precipitated as Sb_2O_3 in the temperature range 580 to 420 °C and virtually all precipitated above 273 °C. A similar study by Wan et al. (2023) shows that the As_2O_3

condensation temperature is also sensitive to the O_2 concentration, and over a range of 0.5 to 5 vol% O_2 they noted that As_2O_3 precipitation occurred at temperatures below 250 °C. The Giant Mine roaster operated at temperatures between 450 and 500 °C, so it's possible that Sb vapour began condensing on the surface of calcine and primary-mineral particles, possibly in the roaster, but certainly upstream from the onset of As_2O_3 precipitation. This condensation pathway would have been most important prior to installation of the second ESP (1955) when the mass and surface area of calcine and mineral-dust particles in the gas stream were highest, resulting in less Sb available to substitute in As_2O_3 that condensed downstream at lower temperature. This inference is supported in a report on the mineralogy of the ATRW by CANMET (2004) which states material from chamber B233 "*has the highest bulk antimony content of all the samples, [and] appears to have a lower average antimony content in the arsenic trioxide grains*." After 1955, the lower dust content in the gas stream appears to have caused Sb vapour and condensed particulates to persist in the gas stream and combine with the precipitated As_2O_3.

There are several possible alternative explanations for the As_2O_3 extraction yields that are less than 100% (observation D). First, the presence of relatively large As_2O_3 crystals in the ATRW could prolong the dissolution time beyond the one- and four-minute extraction times. A report on the mineralogy of the ATRW by CANMET (2004) states that all As_2O_3 is similar, occurring as euhedral crystals with grain size < 10 μm, but the report also mentions the relatively rare occurrence of As_2O_3 grains > 30 μm (Figure 18). It's possible that the relatively low extraction yields are from ATRW containing more of the large grains. A second possible explanation is that As_2O_3 may have reprecipitated during the cooling stage of the microwave extractions (Figure 6), but this is unlikely because, even with the lowest W:S ratio (20), the As concentrations in the extraction solutions were well below the solubility curve (Figure *19*).

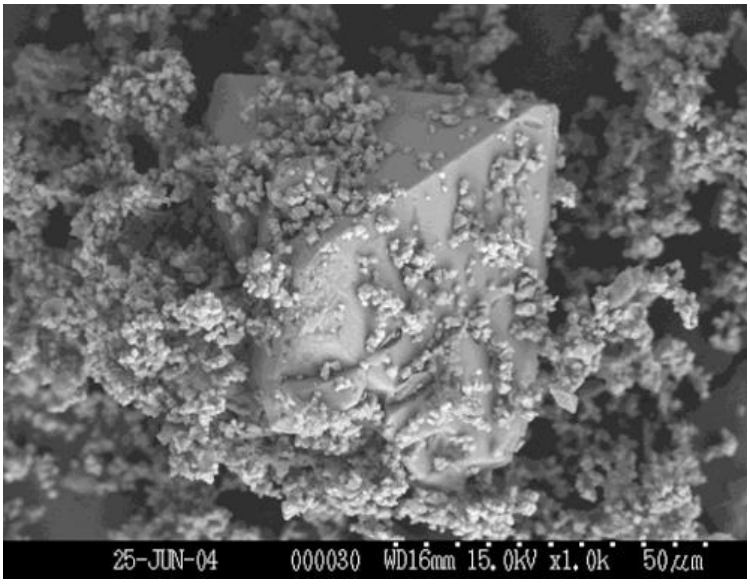

Figure 18. A large As_2O_3 crystal surrounded by smaller As_2O_3 crystals present in ATRW. Figure obtained from Poirier (2004).

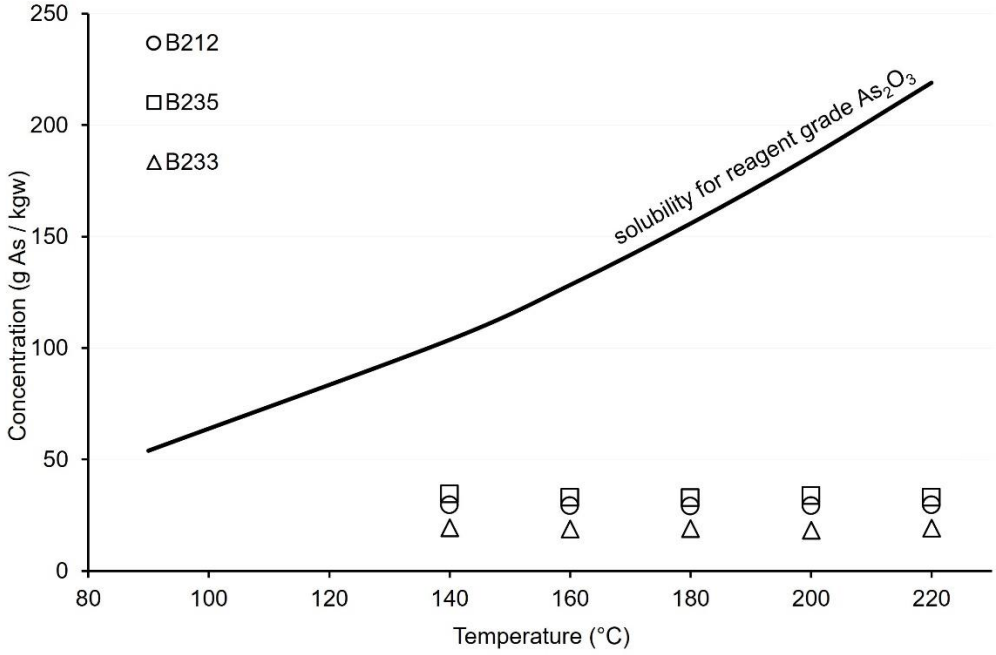

Figure 19. Solubility of reagent grade As_2O_3 (Dutrizac et al., 2000) and estimated concentration of As in extraction solutions (W:S = 20) from chambers B212, B235 and B233.

Little is known about the operating conditions in the Giant Mine roasters over time, but observations E, F and G suggest that, compared to later years, the conditions may have been relatively oxidizing when the ATRW in chamber B233 was produced. Manipulation of the oxidation state in the roaster is mentioned in a description of the early roasting and dust-collection process (Royal Oak Mines, 1995) with a goal of maintaining conditions sufficiently oxidizing to produce SO_3 in the exhaust gas because adsorption of SO_3 on the As_2O_3 particles improved As collection in the ESP. The XANES data for extraction residues from chamber B233 are consistent with a relatively high oxidation state because, unlike data from chambers B212 and B235, the spectra indicate all As is As(V) and linear combination fitting of the Sb spectra indicate that a small fraction (11%) of the Sb is Sb(V). The unique occurrence of scorodite in ATRW from chamber B233 is also consistent with relatively oxidizing conditions because enhanced production of As(V) in the roaster could promote formation of anhydrous $FeAsO_4$ which easily hydrates to form scorodite (Majzlan et al., 2012). According to Foster (1963) and Royal Oak Mines (1995), adjustments to roaster and dust-collection processes stabilized in 1958, suggesting that less variation in the ATRW material properties might be expected for ATRW produced since that time. However, it's likely that variations through time in the mineralogy of the ore also influenced the composition of the ATRW.

3 Conclusions

This research developed a method to completely extract As_2O_3 from Giant Mine ATRW into pure water, resulting in an As-rich extraction solution that is amenable to sulfidation. This removes one of the principal technical barriers toward the transformation of ATRW to thermodynamically stable and low-solubility As_2S_3 that could be permanently and safely be disposed of underground on the Giant Mine site.

In an effort to optimize the energy and water requirements for the extractions, the method was tested at various W:S ratios (20 – 100), temperatures (140 – 220 °C) and times (one and four minutes). Complete As_2O_3 dissolution was achieved at all temperatures and times and a W:S ratio of 100, indicating that high temperature (energy) conditions are not necessary. It was also demonstrated that, with the exception of As, the major-ion concentrations in the extraction solutions are low (< 200 mg/L) and could therefore be recycled numerous times during the As_2O_3 extraction / As_2S_3 precipitation cycle.

The characterization of extraction residues determined that 1 – 14% of the total As remained in the residues after extraction of As_2O_3, primarily as As(V) with lesser As(III); both associated with Fe minerals. In addition, 23 – 93% of the bormstadtotal Sb remained in the residue, primarily as Sb(III) with lesser Sb(V). It is recognized that the chemical and mineralogical properties of the ATRW evolved through time in response to changes in the configuration of the roaster and dust-collection system. As a consequence, As_2O_3 produced after ~1958 should be expected to contain a higher Sb-impurity content, which has been shown to reduce the As_2O_3 extraction yield in water.

4 References

Ali M. and Ahmed M. (2003) Environmental chemistry of arsenic. *Arsenic contamination: Bangladesh Perspective. ITN-Bangladesh, Dhaka*, 21–41.

Bailey A. S., Jamieson H. E. and Radková A. B. (2021) Geochemical characterization of dust from arsenic-bearing tailings, Giant Mine, Canada. *Applied Geochemistry* **135**. Doi:10.1016/j.apgeochem.2021.105119

Ball J. W. and Nordstrom D. K. (1991) *User`s manual for wateq4f, with revised thermodynamic data base and test cases for calculating speciation of major, trace, and redox elements in natural waters*., USGS open-file report 91-183, California.

Bank of Canada (2025) Inflation calculator. *https://www.bankofcanada.ca/rates/related/*.

Bromstad M. J., Wrye L. A. and Jamieson H. E. (2017) The characterization, mobility, and persistence of roaster-derived arsenic in soils at Giant Mine, NWT. *Applied Geochemistry* **82**, 102–118.

Bromstad M. and Jamieson H. E. (2012) Giant Mine, Yellowknife, Canada: arsenite waste as the legacy of gold mining and processing. In *The Metabolism of Arsenite* CRC Press. pp. 25–42.

CANMET (2004) *A mineralogical investigation of arsenic trioxide rich tailings from the Giant Mine, Yellowknife, NWT.*, Ottawa, ON.

Clark I. D. and Raven K. G. (2004) Sources and circulation of water and arsenic in the Giant Mine, Yellowknife, NWT, Canada. *Isotopes Environ. Health Stud.* **40**, 115–128.

Crown-Indigenous Relations and Northern Affairs Canada (2024) The remediation project's frozen block method. *https://www.rcaanc-cirnac.gc.ca/eng/1100100027422/1617999507283*.

Deng T. (1993) Aqueous pressure oxidation of minerals - a salient development in hydrometallurgy. *Mineral Processing and Extractive Metallurgy Review* **12**, 185–222.

Dutrizac J. E., Riveros P. A., Chen T. T. and Dubreuil A. (2000) *Recovery and purification of arsenic oxide - Giant Mine*., Report MMSL 2000-004 (CR), Ottawa, ON.

Fodje M., Grochulski P., Janzen K., Labiuk S., Gorin J. and Burg R. (2014) 08B1-1: an automated beamline for macromolecular crystallography experiments at the Canadian Light Source. *J. Synchrotron Radiat.* **21**, 633–637.

Foster E. O. (1963) The collection and recovery of gold from roaster exit gases at Giant Yellowknife. *The Canadian Mining and Metallurgical Bulletin* **LXVI**, 245–251.

Fraser K. S., Walton R. H. and Wells J. A. (1991) Processing of refractory gold ores. *Miner. Eng.* **4**, 1029–1041.

Geldart J., Williamson R. and Maltby P. (1992) Aqueous pressure oxidation as a waste treatment process—stabilizing roaster wastes. *Hydrometallurgy* **30**, 29–44.

Government of Canada (2017) Water sources: groundwater. *https://www.canada.ca/en/environment-climate-change/services/water-overview/sources/groundwater.html*.

Han F. X., Su Y., Monts D. L., Plodinec M. J., Banin A. and Triplett G. E. (2003) Assessment of global industrial-age anthropogenic arsenic contamination. *Naturwissenschaften* **90**, 395–401.

Health Canada (2025) Arsenic in drinking water. *https://www.canada.ca/en/health-canada/services/healthy-living/your-health/environment/arsenic-drinking-water.html*.

INAC and Government of the Northwest Territories (2010) *Giant Mine remediation project developer's assessment report*., Yellowknife, NWT.

Jamieson H. E. (2014) The legacy of arsenic contamination from mining and processing refractory gold ore at Giant Mine, Yellowknife, Northwest Territories, Canada. *Rev. Mineral. Geochem.* **79**, 533–551.

Ko I., Ahn J. S., Park Y. S. and Kim K. W. (2003) Arsenic contamination of soils and sediments from tailings in the vicinity of Myungbong Au mine, Korea. *Chemical Speciation and Bioavailability* **15**, 67–74.

Kyle J. and Lunt D. (1991) Investigation of disposal options for arsenic trioxide produced from roasting operations. In *AusIMM Extractive Metallurgy Conference* Perth, Aust. pp. 347–353.

Lee P. K., Yu S., Jeong Y. J., Seo J., Choi S. G. and Yoon B. Y. (2019) Source identification of arsenic contamination in agricultural soils surrounding a closed Cu smelter, South Korea. *Chemosphere* **217**, 183–194.

Lemos F. de A., Nascimento M., Moreira Júnior G. R., Andrade V. R. de, Pinto P. C. and Salles A. J. G. (2025) Recovery of gold from refractory ore employing pressure oxidation. *REM - International Engineering Journal* **78**, 1-12.

Lengke M. F. and Tempel R. N. (2002) Reaction rates of natural orpiment oxidation at 25 to 40°C and pH 6.8 to 8.2 and comparison with amorphous As2S3 oxidation. *Geochim. Cosmochim. Acta* **66**, 3281–3291.

Li L., Zhang B., Jiang B., Zhao Y., Qian G. and Hu X. (2022) Potentially toxic elements in weathered waste-rocks of Fushun western opencast mine: distribution, source identification, and contamination assessment. *Environ. Geochem. Health* **44**, 1813–1826.

Lum J. E., Schoepfer V. A., Jamieson H. E., McBeth J. M., Radková A. B., Walls M. P. and Lindsay M. B. J. (2023) Arsenic and antimony geochemistry of historical roaster waste from the Giant Mine, Yellowknife, Canada. *J. Hazard. Mater.* **458**. Doi:10.1016/j.jhazmat.2023.132037

MacGregor D., Jordan-Knox Q. and Royle M. (2004) *Giant Mine arsenic trioxide management project: arsenic trioxide chamber drilling and testing program (No. 1C1001.012.B66).* SRK Consulting., Vancouver, BC.

Mackenzie Valley Review Board (2013) *Environmental assessment and reasons for decision Giant Mine remediation project*., Yellowknife, NWT. EA0809-001_Giant_Report_of_Environmental_Assessment_June_20_2013.PDF

Majzlan J., Drahota P., Filippi M., Grevel K. D., Kahl W. A., Plášil J., Boerio-Goates J. and Woodfield B. F. (2012) Thermodynamic properties of scorodite and parascorodite (FeAsO4•2H2O), kaňkite (FeAsO4•3.5H2O), and FeAsO4. *Hydrometallurgy* **117–118**, 47–56.

Mohammadi A., Demers I. and Beier N. (2024a) Geomechanical aspects of stabilizing arsenic trioxide roaster waste in cemented paste backfill at the Giant Mine, Canada. *J. Environ. Manage.* **370**. Doi: 10.1016/j.jenvman.2024.123022

Mohammadi A., Schoepfer V. A., Demers I. and Beier N. A. (2024b) Study on the leaching behavior of cemented paste backfill containing arsenic trioxide roaster waste. *Discover Civil Engineering* **1**. Doi: 10.1007/s44290-024-00137-0

Moore J. W. and Ramamoorthy S. (2012) Heavy metals in natural waters: applied monitoring and impact assessment. In Springer Science & Business Media, New York, NY. pp. 4–22.

Murcott S. (2012) *Arsenic contamination in the world*., IWA Publishing, London, UK.

Nazari A. M., Radzinski R. and Ghahreman A. (2017) Review of arsenic metallurgy: treatment of arsenical minerals and the immobilization of arsenic. *Hydrometallurgy* **174**, 258–281.

Ng W. S., Liu Y., Wang Q. and Chen M. (2023) The fate of the arsenic species in the pressure oxidation of refractory gold ores: practical and modelling aspects. *Mineral Processing and Extractive Metallurgy Review* **44**, 155–187.

Nickson R., McArthur J., Burgess W., Ahmed K. M., Ravenscroft P. and Rahman M. (1998) Arsenic poisoning of Bangladesh groundwater. *Nature* **395**, 338.

Nordstrom K., Majzlan J. and Konigsberger E. (2014) Thermodynamic properties for arsenic minerals and aqueous species. *Reviews in Minerology & Geochemistry* **79**, 217–255.

Northwest Consulting Limited (2003) *An examination of arsenic contamination in the roaster and gas handling complex at the Giant mill*., Vancouver, BC.

Parsons J. G., Lopez M. L., Castillo-Michel H., Peralta-Videa J. R. and Gardea-Torresdey J. L. (2009) Arsenic speciation in biological samples using XAS and mixed oxidation state calibration standards of inorganic arsenic. *Appl. Spectrosc.* **63**, 961-969.

Poirier G. (2004) *Mineralogy of Giant Mine As2O3 waste*., CANMET Report 04-028(CR), Ottawa, ON.

Pokrovski G., Gout R., Schott J., Zotov A. and Harrichoury J.-C. (1996) Thermodynamic properties and stoichiometry of As (III) hydroxide complexes at hydrothermal conditions. *Geochim. Cosmochim. Acta* **60**, 737–749.

Qin H., Guo X., Tian Q., Yu D. and Zhang L. (2021) Recovery of gold from sulfide refractory gold ore: oxidation roasting pretreatment and gold extraction. *Miner. Eng.* **164**. Doi: 10.1016/j.mineng.2021.106822

Rae I. D. (2020) Arsenic: its chemistry, its occurrence in the earth and its release into industry and the environment. *ChemTexts* **6**. Doi: 10.1007/s40828-020-00118-7

Riveros P. A., Dutrizac J. E. and Spencer P. (2001) Arsenic disposal practices in the metallurgical industry. *Canadian Metallurgical Quarterly* **40**, 395–420.

Rodríguez V. M., Jiménez-Capdeville M. E. and Giordano M. (2003) The effects of arsenic exposure on the nervous system. *Toxicol. Lett.* **145**, 1–18.

Rong Z., Tang X., Wu L., Chen X., Dang W. and Wang Y. (2020) A novel method to synthesize scorodite using ferrihydrite and its role in removal and immobilization of arsenic. *Journal of Materials Research and Technology* **9**, 5848–5857.

Royal Oak Mines (1995) *Arsenic emissions from gold roasters*., Vancouver, BC.

Royal Oak Mines (1997) Longitudinal cross section. *https://data.gmob.ca/dataset/giant-mine-internal-operation-and-administration-1964-1999-electronic-resources-series-1/resource/391dd74e-ecee-4761-bbf3-f01068d6292f*.

Sandlos J. and Keeling A. (2016) Toxic legacies, slow violence, and environmental injustice at Giant Mine, Northwest Territories. *The Northern Review* **42**, 7–21.

Schwertmann U. and Cornell R. M. (2000) *Iron oxides in the laboratory*., WILEY-VCH, Baden, Switzerland.

SRKa (2002) *Arsenic trioxide management alternatives*., Vancouver, BC.

SRKb (2002) *Giant Mine hydrogeology: supporting document 2*., Vancouver, BC.

SRK (2007) *Giant Mine remediation plan*., Vancouver, BC.

Tennant E. (2023) Investigating the high-temperature (100 °C – 200 °C) dissolution and sulfidation of As2O3 stored at the Giant Mine, NWT, Canada. Master`s Thesis, University of Ottawa.

Thienpont J. R., Korosi J. B., Hargan K. E., Williams T., Eickmeyer D. C., Kimpe L. E., Palmer M. J., Smol J. P. and Blais J. M. (2016) Multi-trophic level response to extreme metal contamination from gold mining in a subarctic lake. *Proceedings of the Royal Society B: Biological Sciences* **283**. Doi: 10.1098/rspb.2016.1125

Toby B. H. and Von Dreele R. B. (2013) GSAS-II: the genesis of a modern open-source all purpose crystallography software package. *J. Appl. Crystallogr.* **46**, 544–549.

Tuominen J., Sukhomlinov D., Taskinen P. and Lindberg D. (2025) Antimony vaporization and condensation in simulated flash smelting off-gas train conditions. *Metallurgical and Materials Transactions B: Process Metallurgy and Materials Processing Science* **56**, 307–320.

Walker S. R., Jamieson H. E., Lanzirotti A., Andrade C. F. and Hall G. E. M. (2005) The speciation of arsenic in iron oxides in mine wastes from the Giant gold Mine, N.W.T.: application of synchrotron micro-xrd and micro-xanes at the grain scale. *The Canadian Mineralogist* **43**, 1205–1224.

Walker S. R., Jamieson H. E., Lanzirotti A., Hall G. E. M. and Peterson R. C. (2015) The effect of ore roasting on arsenic oxidation state and solid phase speciation in gold mine tailings. *Geochemistry: Exploration, Environment, Analysis* **15**, 273–291.

Wan X., Sukhomlinov D., Taskinen P., Lindgren M., Michallik R. and Jokilaakso A. (2023) Arsenic condensation and reaction mechanisms in flash smelting off-gas line conditions. *Metallurgical and Materials Transactions B: Process Metallurgy and Materials Processing Science* **54**, 2747–2757.

York G. and Schlaefli S. (2025) In Namibia, a Canadian copper company leaves a legacy of toxic waste. *The Globe and Mail*.

Yunus F. M., Khan S., Chowdhury P., Milton A. H., Hussain S. and Rahman M. (2016) A Review of groundwater arsenic contamination in Bangladesh: The millennium development goal era and beyond. *Int. J. Environ. Res. Public Health* **13**. Doi: 10.3390/ijerph13020215

Zueter A. F. and Sasmito A. P. (2023) Cold energy storage as a solution for year-round renewable artificial ground freezing: case study of the Giant Mine remediation project. *Renew. Energy* **203**, 664–676.

5 Appendices

Table A- 1. Elemental concentrations (ppm) in As_2O_3 extraction solutions: extraction time of one minute and W:S = 100.

Chamber	Temp (°C)	Al	As	Ca	Cu	Fe	K	Mg	Mn	Na	Ni	Pb	S	Sb	Si	Zn
B212	140	0.0649	5823.3946	35.6771	LD	0.0744	1.4493	17.5803	0.0636	1.2325	LD	LD	24.5838	103.8928	0.2451	0.0521
	160	0.0473	5814.5237	39.4511	0.0284	0.0667	1.4607	18.9232	0.0803	1.3671	LD	LD	24.4082	127.8270	2.1614	0.0649
	180	LD	5802.2863	41.0099	LD	0.0655	1.4493	19.4899	0.0965	0.8560	LD	LD	25.1129	131.7715	2.4260	0.0587
	200	0.0413	5776.5739	42.1964	0.0645	0.1132	1.4607	20.3785	0.1172	0.9121	LD	LD	25.0852	138.9149	7.9650	0.1462
	220a	0.0875	5823.3176	41.7669	LD	0.2896	1.5307	20.5659	0.1421	1.0740	LD	LD	25.9033	137.9182	14.7136	0.1906
	220b	0.0425	5729.4064	41.6703	LD	0.1570	1.6402	20.4421	0.1354	1.8190	LD	LD	25.3472	137.1393	15.1697	0.1021
	220c	0.1677	5702.1392	40.5368	LD	0.1491	1.7318	20.2192	0.1213	2.9144	LD	LD	24.5030	137.3994	25.6119	0.0865
B233	140	2.1998	3836.4475	54.5590	0.9774	1.5421	3.7051	49.9570	0.4502	2.0669	0.4688	LD	90.5396	8.2992	0.1863	2.4541
	160	1.6129	3751.4056	54.1259	0.9059	3.2910	3.7950	48.2088	0.5584	2.1509	0.4642	LD	88.5379	9.5933	0.5680	2.6875
	180	1.3856	3811.1060	56.2956	0.4619	4.6873	4.0681	48.6223	0.6142	2.7513	0.4528	LD	90.3099	10.7165	1.4071	2.7202
	200	1.2256	3575.8362	56.0815	0.0634	6.9501	4.0332	45.7232	0.6683	2.4904	0.4087	LD	84.8314	10.9484	3.3813	2.7575
	220a	1.3438	3806.5323	53.9520	0.0458	7.4211	4.6212	48.0536	0.6946	4.8990	0.3917	LD	93.0225	11.5008	14.6861	3.1012
	220b	1.2566	3797.3894	53.4998	0.0656	5.8047	4.4832	47.6369	0.6694	2.9799	0.3960	LD	92.0211	11.8269	12.7201	2.9669
	220c	1.2012	3788.2543	53.1843	0.0582	6.5765	4.4296	47.9866	0.6798	3.2470	0.3840	LD	91.7489	11.9131	12.2284	3.0234
B235	140	0.0888	6819.1373	19.6737	LD	0.0699	1.1476	16.4051	0.0923	0.9107	LD	LD	15.2433	22.2477	0.2612	0.0183
	160	LD	6490.1599	20.9302	LD	0.0586	1.5601	16.3929	0.0853	3.4193	LD	LD	15.5390	23.6229	1.2985	0.2948
	180	LD	6557.3150	21.0264	LD	0.0229	1.5870	17.1087	0.1085	3.1761	LD	LD	15.1737	24.6732	1.7813	0.3423
	200	LD	6561.2865	22.0951	0.0163	0.0442	1.4357	17.7191	0.1285	3.1132	LD	LD	15.0173	23.8535	4.3599	0.2266
	220a	LD	6524.7652	23.3078	LD	0.0270	1.5272	17.7238	0.1649	2.6440	LD	LD	16.6087	24.7276	12.8002	0.2287
	220b	LD	6538.1276	19.7975	LD	0.0267	1.5487	17.6845	0.1541	2.9931	LD	LD	15.4251	24.6517	16.0363	0.2342
	220c	0.0391	6554.1919	19.8601	LD	0.0308	1.5249	17.5964	0.1600	2.7975	LD	LD	14.9482	24.7692	13.2798	0.2343

Table A- 2. Elemental composition (ppm) of residues: extraction time of one minute and W:S = 100.

Chamber	Temp (°C)	As	Cu	Fe	Mn	Ni	Pb	S	Sb	Zn
B212	140	103617.5075	1426.1734	167915.1095	640.4509	396.2127	6521.3092	2551.9799	37018.3756	3197.2665
	160	93739.0258	1470.5917	176905.5770	659.0146	414.7510	6826.5975	2666.4555	33961.6796	3291.5219
	180	92801.1080	1527.0816	188938.3615	673.0400	458.3647	7143.1278	2816.2777	33255.4847	3411.0357
	200	85019.6516	1475.2408	181237.7499	666.6592	430.0777	7150.6161	2798.7111	31281.8388	3419.9764
	220a	89881.9900	1579.2383	194942.2364	676.5603	446.0758	7442.5742	2833.1195	33407.4481	3517.7062
B233	140	173269.4263	1291.3300	211011.9339	458.4681	279.0585	8865.9813	4409.7183	29291.3204	3202.5156
	160	167086.2294	1371.7717	217051.4016	463.7925	298.0789	9525.0820	4738.9994	30716.0788	3372.6240
	180	165497.5076	1505.9240	217367.2695	447.4669	301.5515	9416.2600	4619.4694	29779.1426	3349.8757
	200	162426.0490	1660.1235	222906.2929	430.7026	303.4241	9701.3416	4609.8260	30765.5257	3364.3235
	220a	154988.1615	1635.9994	225288.1064	435.9682	326.0760	9841.2952	4483.7360	31223.4079	3322.0171
	220b	154400.1893	1565.7202	223529.9392	421.4693	321.8502	9310.4522	4533.1660	29966.2019	3287.5091
	220c	159215.1949	1621.2222	225057.5251	443.3045	324.9406	9824.6962	4433.1576	30936.7561	3331.3017
B235	140	106811.1191	1746.7922	146707.7917	701.3691	402.0174	2908.0503	1445.3737	10187.4864	2289.8737
	160	106265.0486	1844.1265	136580.4063	757.5184	390.5031	3165.4600	1295.6949	9899.6010	2374.6770
	180	104278.4898	1923.9410	139442.1152	773.7363	400.2233	3322.3135	1295.0040	9945.9668	2462.6410
	200	101305.8698	2019.6390	144536.2674	788.6583	420.5618	3451.0923	1525.2281	10407.6017	2532.0430
	220a	96843.8682	2174.2789	148116.0166	815.8271	447.5887	3674.7696	1500.4700	9526.2350	2652.1992

Table A- 3. Extractable mass fraction (%) for extraction time of one minute and W:S = 100

Chamber	Temp (°C)	As	Cu	Fe	Mn	Ni	Pb	S	Sb	Zn
212	140	96.1290	LD	0.0196	4.2036	LD	LD	80.9763	55.3592	0.7147
	160	96.7214	0.9113	0.0179	5.4787	LD	LD	81.3206	64.1585	0.9288
	180	96.6804	LD	0.0162	6.2586	LD	LD	80.5964	64.8598	0.7954
	200	97.2274	2.2058	0.0322	8.3154	LD	LD	82.2253	69.6227	2.1587
	220	96.9052	LD	0.0717	9.2165	LD	LD	81.5456	66.6134	2.5523
233	140	83.5858	14.8263	0.1678	18.4239	27.8706	LD	82.5239	6.1177	14.9836
	160	84.0738	13.4397	0.3552	22.0624	26.8038	LD	81.4566	6.8410	15.7796
	180	85.3141	7.1820	0.5410	25.7207	27.4741	LD	83.1416	8.3227	17.0019
	200	86.2370	1.0752	0.8796	30.6335	27.7129	LD	83.9681	9.1970	18.9152
	220	86.5149	0.7265	0.8531	29.3863	23.8859	LD	84.4223	8.7772	19.6051
235	140	98.1954	LD	0.0406	10.0900	LD	LD	89.9888	65.0511	0.6758
	160	98.5855	LD	0.0572	11.1064	LD	1.2037	93.0164	69.1843	11.0144
	180	98.5613	LD	0.0249	12.7874	LD	2.3411	92.6544	68.8804	14.9758
	200	98.7232	0.3241	0.0386	16.2012	LD	LD	92.0853	69.0083	9.5531
	220	98.9199	LD	0.0257	20.9137	LD	LD	93.3774	77.8065	10.5865

Table A- 4. Certified reference material concentrations (ppm) used to determine precision and accuracy on ICP-OES.

	Al	As	Ca	Cu	Fe	K	Mg	Mn	Na	Ni	S	Pb	Sb	Si	Zn
Extraction Solutions	0.0398	0.4543	0.8310	0.0094	0.0105	0.0944	1.3294	0.0419	0.4330	0.0042	1.8698	N/A	0.0445	0.0083	0.0105
Digested Residues	N/A	0.4377	N/A	0.8433	1.2890	N/A	N/A	0.3447	N/A	0.8393	0.1119	2.0348	0.0430	N/A	0.8803

Table A- 5. Elemental mass (mg) in As_2O_3 extraction solutions: extraction time of one minute and W:S = 100.

	Temp(°C)	Al	As	Ca	Cu	Fe	K	Mg	Mn	Na	Ni	Pb	S	Sb	Si	Zn
B212	140	0.0013	118.6225	0.7267	0.0000	0.0015	0.0295	0.3581	0.0013	0.0251	0.0000	0.0000	0.5008	2.1163	0.0050	0.0011
	160	0.0009	116.6975	0.7918	0.0006	0.0013	0.0293	0.3798	0.0016	0.0274	0.0000	0.0000	0.4899	2.5655	0.0434	0.0013
	180	0.0000	116.2198	0.8214	0.0000	0.0013	0.0307	0.3904	0.0019	0.0171	0.0000	0.0000	0.5030	2.6394	0.0486	0.0012
	200	0.0008	116.5713	0.8515	0.0013	0.0023	0.0331	0.4112	0.0024	0.0184	0.0000	0.0000	0.5062	2.8033	0.1607	0.0030
	220a	0.0018	117.9222	0.8458	0.0000	0.0059	0.0351	0.4165	0.0029	0.0217	0.0000	0.0000	0.5245	2.7928	0.2980	0.0039
	220b	0.0009	114.9892	0.8363	0.0000	0.0032	0.0356	0.4103	0.0027	0.0365	0.0000	0.0000	0.5087	2.7524	0.3045	0.0020
	220c	0.0034	115.7534	0.8229	0.0000	0.0030	0.0367	0.4105	0.0025	0.0592	0.0000	0.0000	0.4974	2.7892	0.5199	0.0018
B233	140	0.0444	77.3811	1.1005	0.0197	0.0311	0.0747	1.0076	0.0091	0.0417	0.0095	0.0000	1.8262	0.1674	0.0038	0.0495
	160	0.0325	75.5908	1.0906	0.0183	0.0663	0.0765	0.9714	0.0113	0.0433	0.0094	0.0000	1.7840	0.1933	0.0114	0.0542
	180	0.0278	76.3365	1.1276	0.0093	0.0939	0.0815	0.9739	0.0123	0.0551	0.0091	0.0000	1.8089	0.2147	0.0282	0.0545
	200	0.0249	72.7683	1.1413	0.0013	0.1414	0.0821	0.9305	0.0136	0.0507	0.0083	0.0000	1.7263	0.2228	0.0688	0.0561
	220a	0.0271	76.6636	1.0866	0.0009	0.1495	0.0931	0.9678	0.0140	0.0987	0.0079	0.0000	1.8735	0.2316	0.2958	0.0625
	220b	0.0253	76.4414	1.0770	0.0013	0.1168	0.0902	0.9589	0.0135	0.0600	0.0080	0.0000	1.8524	0.2381	0.2561	0.0597
	220c	0.0243	76.7879	1.0780	0.0012	0.1333	0.0898	0.9727	0.0138	0.0658	0.0078	0.0000	1.8597	0.2415	0.2479	0.0613
B235	140	0.0018	137.7466	0.3974	0.0000	0.0014	0.0232	0.3314	0.0019	0.0184	0.0000	0.0000	0.3079	0.4494	0.0053	0.0004
	160	0.0000	132.1397	0.4261	0.0000	0.0012	0.0318	0.3338	0.0017	0.0696	0.0000	0.0000	0.3164	0.4810	0.0264	0.0060
	180	0.0000	130.9496	0.4199	0.0000	0.0005	0.0317	0.3417	0.0022	0.0634	0.0000	0.0000	0.3030	0.4927	0.0356	0.0068
	200	0.0000	135.0969	0.4549	0.0003	0.0009	0.0296	0.3648	0.0026	0.0641	0.0000	0.0000	0.3092	0.4911	0.0898	0.0047
	220a	0.0000	131.8655	0.4657	0.0000	0.0005	0.0305	0.3541	0.0033	0.0528	0.0000	0.0000	0.3318	0.4941	0.2557	0.0046
	220b	0.0000	134.2278	0.4064	0.0000	0.0005	0.0318	0.3631	0.0032	0.0614	0.0000	0.0000	0.3167	0.5061	0.3292	0.0048
	220c	0.0008	132.7879	0.4024	0.0000	0.0006	0.0309	0.3565	0.0032	0.0567	0.0000	0.0000	0.3029	0.5018	0.2690	0.0047

Table A- 6. Elemental mass (mg) of residues: extraction time of one minute and W:S = 100.

Chamber	Temp(°C)	As	Cu	Fe	Mn	Ni	Pb	S	Sb	Zn
B212	140	3.3054	0.0455	5.3565	0.0204	0.0126	0.2080	0.0814	1.1809	0.1020
	160	2.8215	0.0443	5.3249	0.0198	0.0125	0.2055	0.0803	1.0222	0.0991
	180	3.3223	0.0547	6.7640	0.0241	0.0164	0.2557	0.1008	1.1905	0.1221
	200	0.9692	0.0168	2.0661	0.0076	0.0049	0.0815	0.0319	0.3566	0.0390
	220	3.1279	0.0550	6.7840	0.0235	0.0155	0.2590	0.0986	1.1626	0.1224
B233	140	5.6313	0.0420	6.8579	0.0149	0.0091	0.2881	0.1433	0.9520	0.1041
	160	4.6784	0.0384	6.0774	0.0130	0.0083	0.2667	0.1327	0.8601	0.0944
	180	5.2463	0.0477	6.8905	0.0142	0.0096	0.2985	0.1464	0.9440	0.1062
	200	5.5062	0.0563	7.5565	0.0146	0.0103	0.3289	0.1563	1.0430	0.1141
	220a	5.0216	0.0530	7.2993	0.0141	0.0106	0.3189	0.1453	1.0116	0.1076
	220b	4.7092	0.0478	6.8177	0.0129	0.0098	0.2840	0.1383	0.9140	0.1003
	220c	5.7158	0.0582	8.0796	0.0159	0.0117	0.3527	0.1592	1.1106	0.1196
B235	140	1.7410	0.0285	2.3913	0.0114	0.0066	0.0474	0.0236	0.1661	0.0373
	160	2.3591	0.0409	3.0321	0.0168	0.0087	0.0703	0.0288	0.2198	0.0527
	180	2.4505	0.0452	3.2769	0.0182	0.0094	0.0781	0.0304	0.2337	0.0579
	200	2.3402	0.0467	3.3388	0.0182	0.0097	0.0797	0.0352	0.2404	0.0585
	220	2.2371	0.0502	3.4215	0.0188	0.0103	0.0849	0.0347	0.2201	0.0613

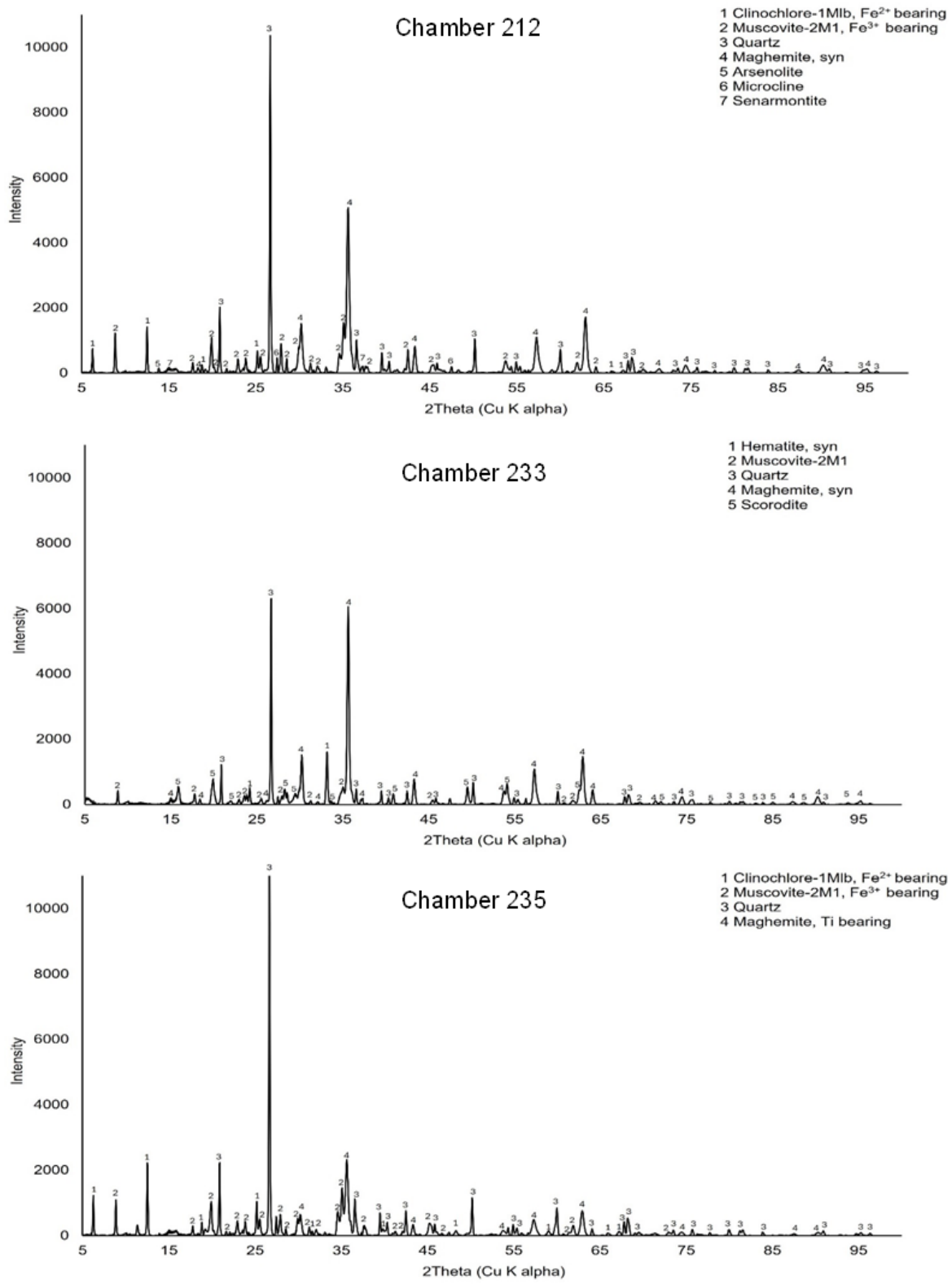

Figure A- 1. pXRD diffraction patterns for As_2O_3 extraction residues.